UCLA Samueli
School of Engineering

SURP 2022 RESEARCH JOURNAL

SUMMER UNDERGRADUATE RESEARCH PROGRAM

TABLE OF CONTENTS

Student Research Abstracts and Posters

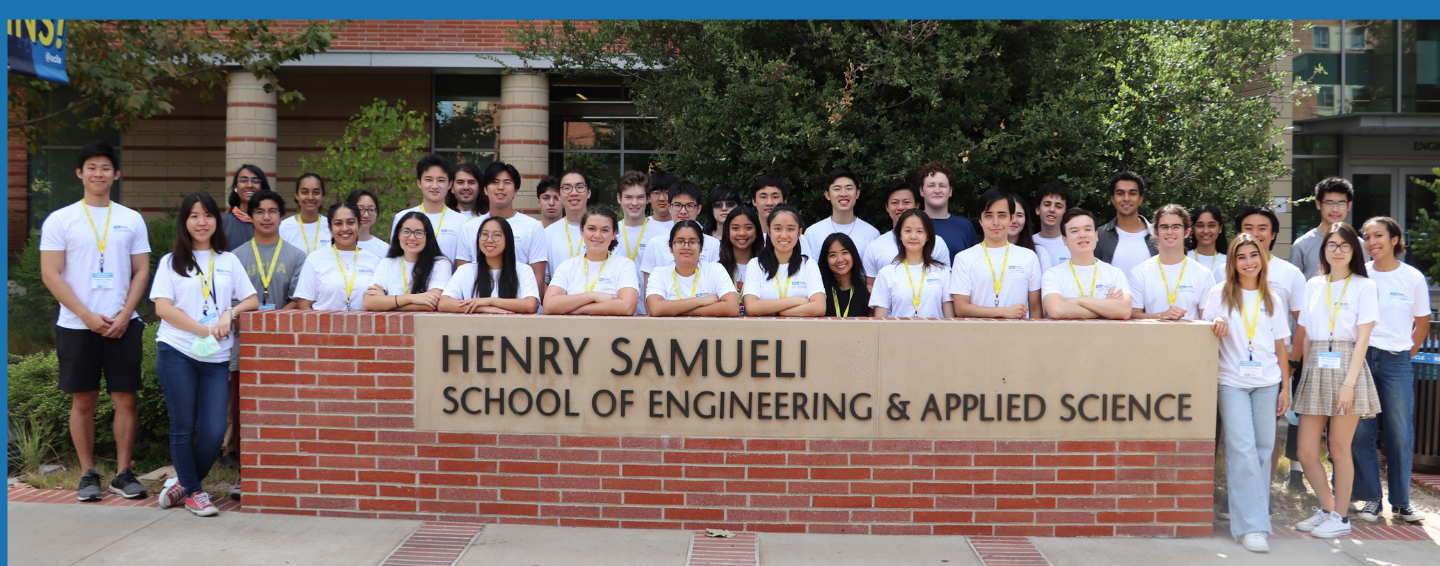

BRUCE DUNN

Interim Dean

INTERIM DEAN'S MESSAGE

The UCLA Samueli School of Engineering's Summer Undergraduate Research Program (SURP) provides a real-world research experience in a wide range of engineering and physical science fields. Through this program, undergraduate students hailing from diverse backgrounds and experiences have an opportunity to conduct research in our faculty's laboratories under their supervision.

In 2022, SURP transitioned back to in-person programming after two years of remote sessions. Students in this year's program have been able to:

- Conduct on-campus research in a cutting-edge field at a world-renowned research institution
- Meet and network with a community of peers who have similar goals and interests
- Create a professional scientific poster and publish a research abstract
- Learn to communicate research outcomes and present a detailed project summary
- Gain a competitive advantage for applying to graduate schools
- Learn how to impact their communities as engineers and scientists

Forty-four undergraduate students were selected to join the 2022 SURP cohort and were mentored by 25 faculty members across six UCLA Engineering departments. UCLA Samueli is committed to fostering a more equitable, diverse and inclusive community. More than 40% of this year's SURP participants are women, 24% are from underrepresented populations, 20% are first-generation students and 18% of the students are from area community colleges.

Creating new knowledge is a challenging but meaningful endeavor, and these high-performing students have done an outstanding job working through the rigors of scholarly research. They should be very proud of all that they have accomplished in a short time this summer. I encourage you to peruse our brochure and learn about their research.

Sincerely,

Bruce Dunn

Bruce Dunn

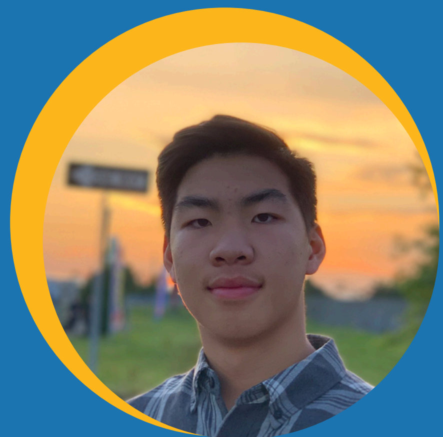

FACULTY ADVISOR
Yang Zhang

DAILY LAB SUPERVISOR
Siyou Pei

DEPARTMENT
Electrical and Computer Engineering

TREVOR CAI

Electrical and Computer Engineering

1st Year, UCLA

Texture Chromeleon - A Toolkit for Quick and Rich Electrovibration Texture Rendering

ABSTRACT

Electrovibration is a principle that revolutionizes the way touchscreens are perceived and interacted with. By applying an oscillating voltage to a screen, electrostatic force is induced between user fingers and the touchscreen, and a wide range of tactile feedback is able to be achieved without the use of any moving parts for superior durability. Additionally, electrovibration can render a richer set of texture than what can be offered by mechanical vibrations. Because of this operating principle, computing devices using electrovibration hold a number of advantages to physical vibration that make it an appealing alternative or addition to its current counterpart. From the lack of wear and tear to increased magnitude and spatial uniformity in tactile feedback, electrovibration induces a perceived sense of friction to sliding fingers that when used in conjunction with physical vibration, allow for a much more immersive experience. Conventionally, designs of electrovibration rely on heuristics that demand experience from the user. Trial and error could also be time consuming. In this project, we propose a toolkit to automate the creation of realistic haptics on conductive materials using electrovibration. Specifically, to use our toolkit, all a user needs is to slide their smartphone with our 3d printed attachment across a real life surface and process the audio with the code provided. By analyzing the audio waveforms generated by different surfaces and applying them using the software platform, Processing, we are able to recreate realistic haptics that replicate the roughness of different surfaces on a conductive surface connected to the electrovibration circuit.

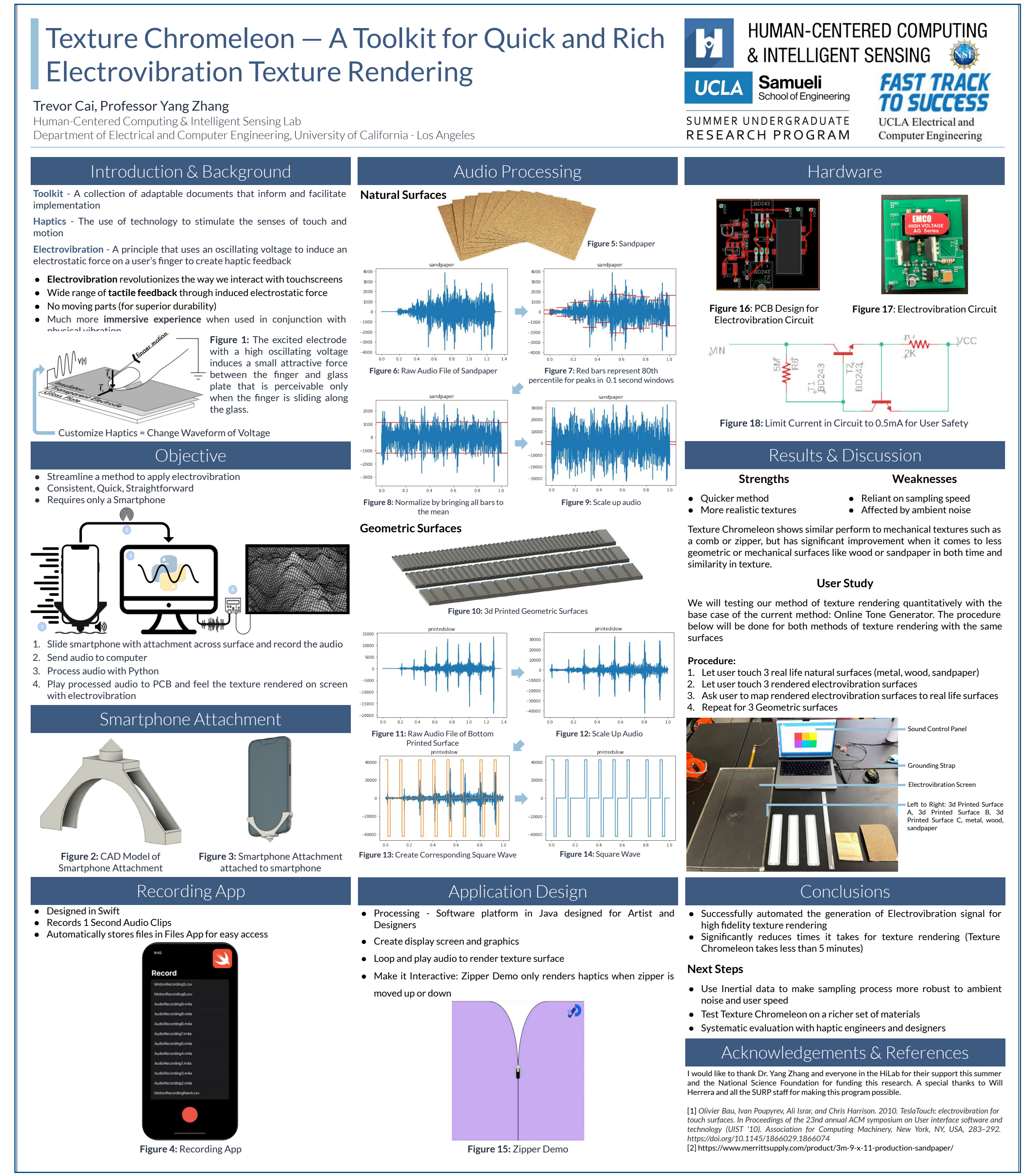

FACULTY ADVISOR

Ankur Mehta

DAILY LAB SUPERVISOR

Ankur Mehta

DEPARTMENT

Electrical and Computer Engineering

DELSIN CARBONELL

Electrical and Computer Engineering

1st Year, El Camino College

Deformable Planar to Spatial Deployable Designs

ABSTRACT

We expect deployable designs to be easy, efficient, and practical to use. Auxetics – elastic geodesic grids in this specific research – can be used as a 2D to 3D deployable design that can form a target curved surface. These grids are built from flat flexible rectangular beams that allow for deformation out of plane, shaping the 3D surface. The structures are relatively simple, cost- efficient, and easy to manufacture. Since elastic geodesic grids require flexible materials to deploy to their 3D state, our objective is to find out what kind of different materials we can use to fabricate them as well as how the materials affect the overall deployment efficiency of the structure. Knowing this, we can determine what surfaces we can and cannot approximate with certain sets of materials. To ensure precise fabrication of the beams and pivot points, we use a laser cutter to create an accurate grid approximation. For future works, we would like to investigate further grid applications such as attaching canvas or membranes over the grids.

FACULTY ADVISOR

Sergio Carbajo

DAILY LAB SUPERVISOR

Brittany Lu

DEPARTMENT

Electrical and Computer Engineering

TIFFANY CHANG

Electrical and Computer Engineering

1st Year, UCLA

A Brighter Future: Next-gen Electron & Photon Probes for Quantum Science Frontiers

ABSTRACT

In the 1900s, photographer Eadweard Muybridge rigged 12 consecutive cameras with a tripwire to produce sequential pictures depicting a horse's motion. These images were monumental in proving that horses amid their gallop are momentarily airborne, but more importantly, they developed the concept known as time-resolved imaging. Today's frontier in sequential motion photography resides on fundamental questions about quantum dynamics utilizing X-ray free electron lasers (XFELs) to understand interactions between light and matter on the femtosecond scale–a quadrillionth of a second. This is game-changing for our basic understanding of nature's smallest, fastest, and most elusive constituents that play a fundamental role in chemistry, biology, and quantum physics. High-quality electron beams are at the heart of these unique sources, which currently rely on decades-old technologies, thus hampering their advancement. Our project explores emerging theories in quantum electrodynamics combined with nonlinear optical techniques (e.g. four-wave mixing) to enhance the quality of electron beams and XFELs dramatically. Through vigorous calculations and computer simulations, we first prove physical theories and follow by building instrumentation informed by this theory. This sparked the design of our hollow-core fiber system, where high-energy light can be tailored to travel according to a wider range of parameters while maintaining its integrity, differing from traditional optical approaches. By completely redesigning the mechanisms of our electron source, we reach the potential for higher peak energies in our beamlines than ever before, creating a generation of unprecedented XFEL technology.

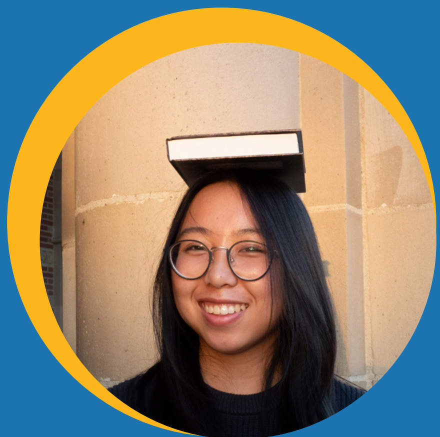

FACULTY ADVISOR

Sanjay Mohanty

DAILY LAB SUPERVISOR

Tonoy Das

DEPARTMENT

Civil and Environmental Engineering

WENDY CHAU

Civil and Environmental Engineering

2nd Year, UCLA

Optimizing Compacted Biofilter Amendments for Stormwater Treatment in Roadside Soils

ABSTRACT

Transportation infrastructures such as roadways in urban areas contribute to pollution via contaminated stormwater runoff. Implementing soil-based stormwater infrastructure such as biofilters could capture and treat the contaminated runoff. However, required compaction for roadside soil limits biofilter's infiltration and treatment capacity. The addition of bulking agents such as sand or large aggregates such as expanded shale, clay, and slate (ESCS) can increase the infiltration capacity. However, the quantity of the bulking agent required to achieve the desired infiltration rate is unknown.

To estimate the optimal amount of bulking agent, we mixed the soil with two bulking agents, sand (0.6 - 0.85 mm), and expanded shale, clay, and slate (ESCS, < 2.8 mm) with different mixing ratios. Further, we amended the soil-bulking agent mixture with biochar to enhance the contaminant removal performance. The result shows that the biofilter media mixture with 50% (v/v) bulking agents, 25% soil, and 25% biochar, meet the required infiltration rate of 1-5 inch.h-1. Under compaction, ESCS-based media exhibited a 3 times higher infiltration rate than sand. While both compacted biofilter media effectively remove E. coli, biofilter amended with sand showed relatively higher removal than ESCS-based media owing to higher straining in sand amended biofilters. The results would help develop design guidelines for roadside stormwater treatment systems that require the compaction of filter media.

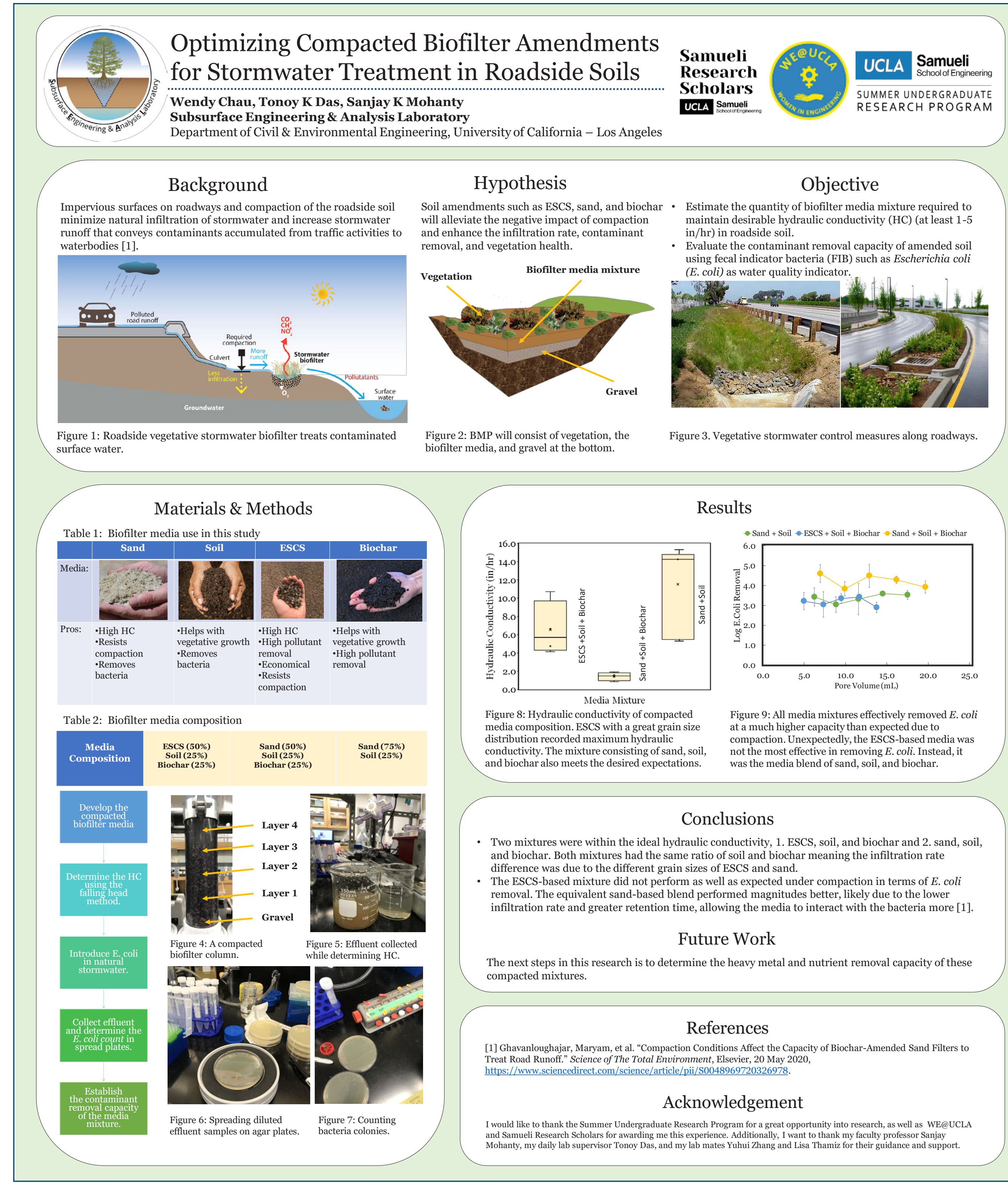

MEGAN CHEN

Electrical and Computer Engineering

1st Year, UCLA

FACULTY ADVISOR

Lara Dolecek

DAILY LAB SUPERVISOR

Lev Tauz

DEPARTMENT

Electrical and Computer Engineering

Methods on Optimizing Sparse Matrix Multiplication

ABSTRACT

Big data and its applications require massive amounts of data computed within the timeframe of milliseconds, and they rely on distributed computations. One such element of distributed computations is large matrix multiplications, and this computation is handled by distributing tasks along worker nodes, as the task is too massive to handle on one machine. Stragglers, nodes that don't finish computations in a timely manner, are bottlenecks for distributed computations. Current solutions mitigating the adverse effect of stragglers inject redundancies in distributed tasks sent to worker nodes, which lowers the recovery threshold, defined as the minimum number of workers needed to recover the result. Here we examine sparsity: the quantity of zero entries in data matrices. Inspiration from previous solutions are applied to lower the recovery threshold when compared to recovery thresholds of non-sparse matrix multiplication. We take advantage of sparsity to directly lower the recovery threshold by compactly packing information from matrices into the shortest possible representation. The results show that improvement in recovery threshold increases as sparsity increases, improving over 70% at high levels of sparsity. While this result demonstrates improvements in tradeoffs between recovery threshold and computation costs, it currently does not account for numerical stability of the algorithms as decimals and errors stemming from finite numerical precision were not explored here. Future work can employ other developed distributed computation methods with sparse matrix multiplications, look into sparsity in multiple matrices, or study the effects of numerical stability.

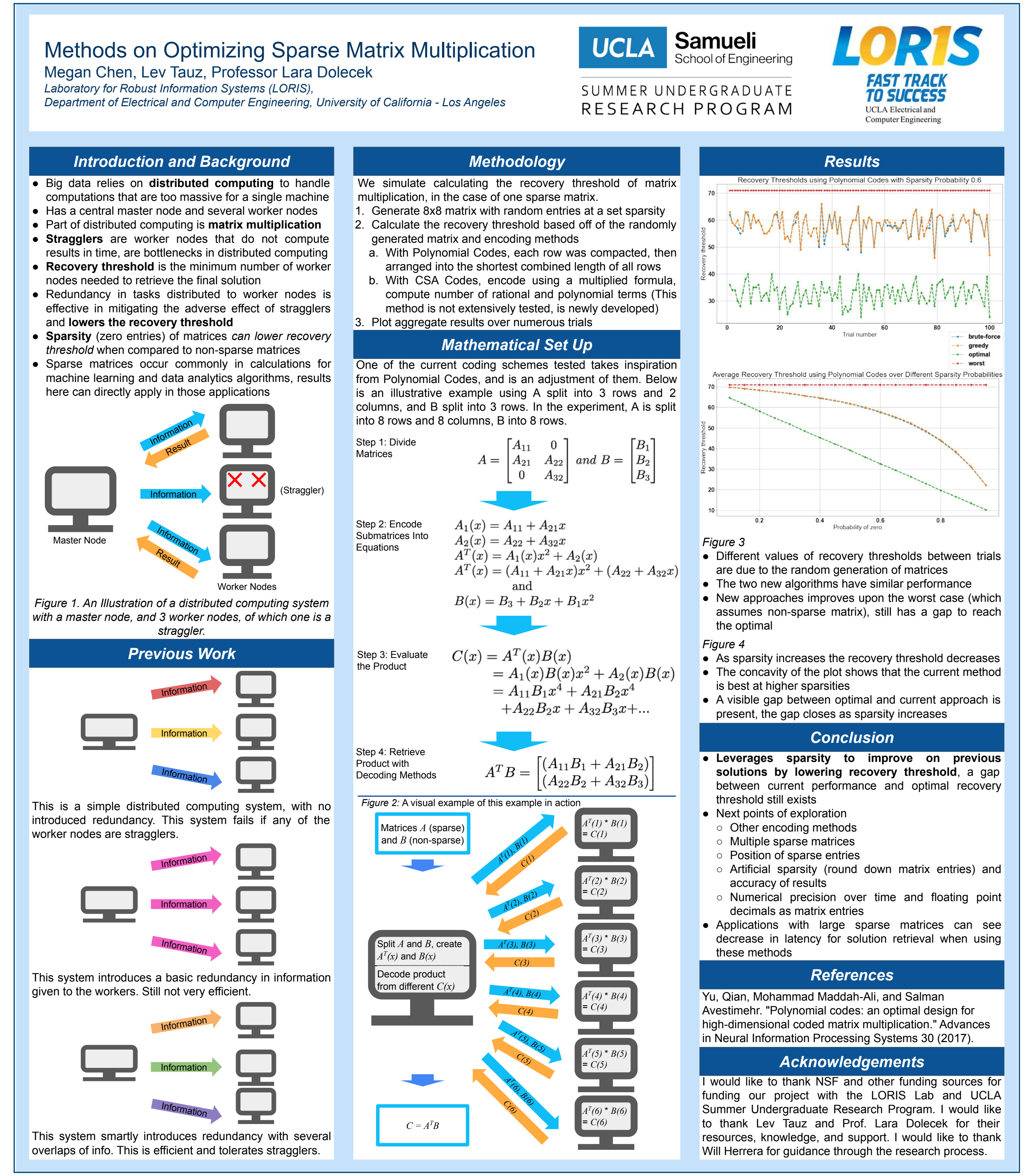

KENNETH CHU

Mechanical and Aerospace Engineering

2nd Year, UCLA

SWETHA PALAKUR

Mechanical and Aerospace Engineering

1st Year, UCLA

FACULTY ADVISOR

Lihua Jin

DAILY LAB SUPERVISOR

Boliang Wu

DEPARTMENT

Mechanical and Aerospace Engineering

BreastBot: A Pneumatically Actuated Soft Robot for Breast Localization in Radiotherapy

ABSTRACT

Radiotherapy is a well-established technique for treating malignant durable cells. In breast radiotherapy, regions of the breast containing cancerous cells are exposed to x-rays to shrink and kill tumors. However, this method of treatment remains unsatisfactory due to crude setups and poor localization techniques that prevent effective normal organ sparing. Overlapping and nearby healthy cells may be unintentionally damaged by radiotherapy in addition to the targeted cancer cells, which results in life-threatening acute and chronic toxicities in breast cancer patients after treatment. To control healthy organ sparing and provide a reproducible setup, this work experimentally develops a pneumatically actuated soft robot to safely isolate the breast from other organs for imaging and treatment using Ecoflex, a silicone elastomer with a low Young's Modulus. We pneumatically actuate the soft robot by pumping air into a network of air channels embedded within the robot's body, causing specific sections of walls to expand and press against the breast. This expansion fixes the breast in a treatable position as far away from the rest of the patient's body as possible. The current working internal pressure of the device is around 5-10 kPa, which is at the 10kPa general comfort limit for patients. Upon actuation, the thickness of the inner wall pressing against the breast is less than 250μm, which minimizes interference with imaging and unwanted radiation exposure. Each device costs less than 5 USD and 4 hours to manufacture excluding the 3D printed mold, so it is practical to custom fit the robot to each patient and dispose of it after treatment. This work demonstrates a promising future for soft robots in medical applications due to their lightweight, adaptable, reproducible, and inexpensive features.

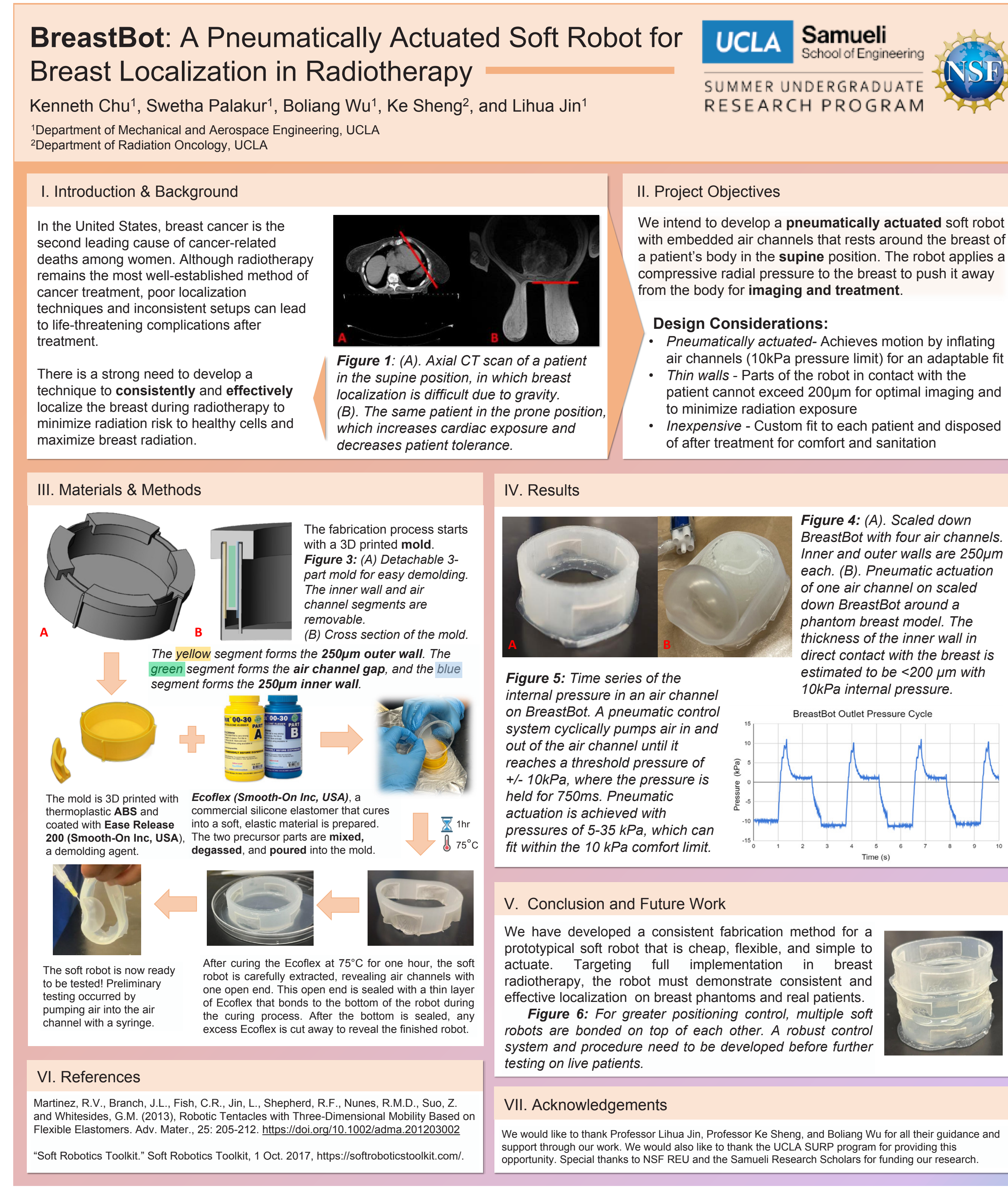

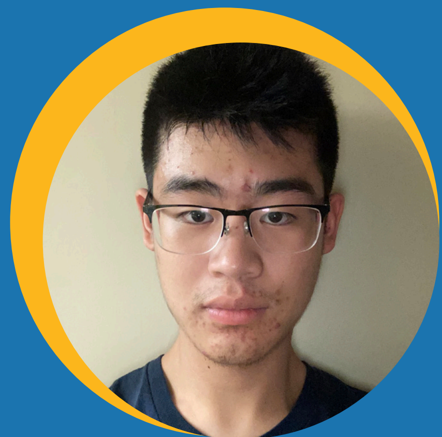

THOMAS CHU

Electrical and Computer Engineering

1st Year, UCLA

FACULTY ADVISOR

Puneet Gupta

DAILY LAB SUPERVISOR

Alexander Graening

DEPARTMENT

Electrical and Computer Engineering

Object Tracking Using Event-Based Cameras and Gabor Filters

ABSTRACT

Event-Based cameras measure the timestamps of discrete changes in pixel intensity and therefore have higher temporal resolution and lower energy use than frame-based cameras. This makes them extremely useful for tracking objects moving extremely quickly, such as aircraft. Convolutional neural networks, which are typically used for frame-based object tracking, require too much computation and are too slow for event-based vision. One solution is to use Gabor filters, which are convolutional filters that are tuned to detect edges, speed, and direction of motion. We wish to benchmark the tracking accuracy of Gabor filters and determine how much accuracy is traded off for speed in their usage. Objects in frame are identified using the density based spatial clustering with noise method. Gabor Filter information is used to predict the future position of these objects. Regions of interest are created around these predicted positions. In future frames, only regions of interest are convolved, significantly speeding up compute time and allowing for the tracking of multiple objects across time. We use the Measure of Tracking Accuracy metric, which utilizes the number of false positives, false negatives, and identity switches across all frames.

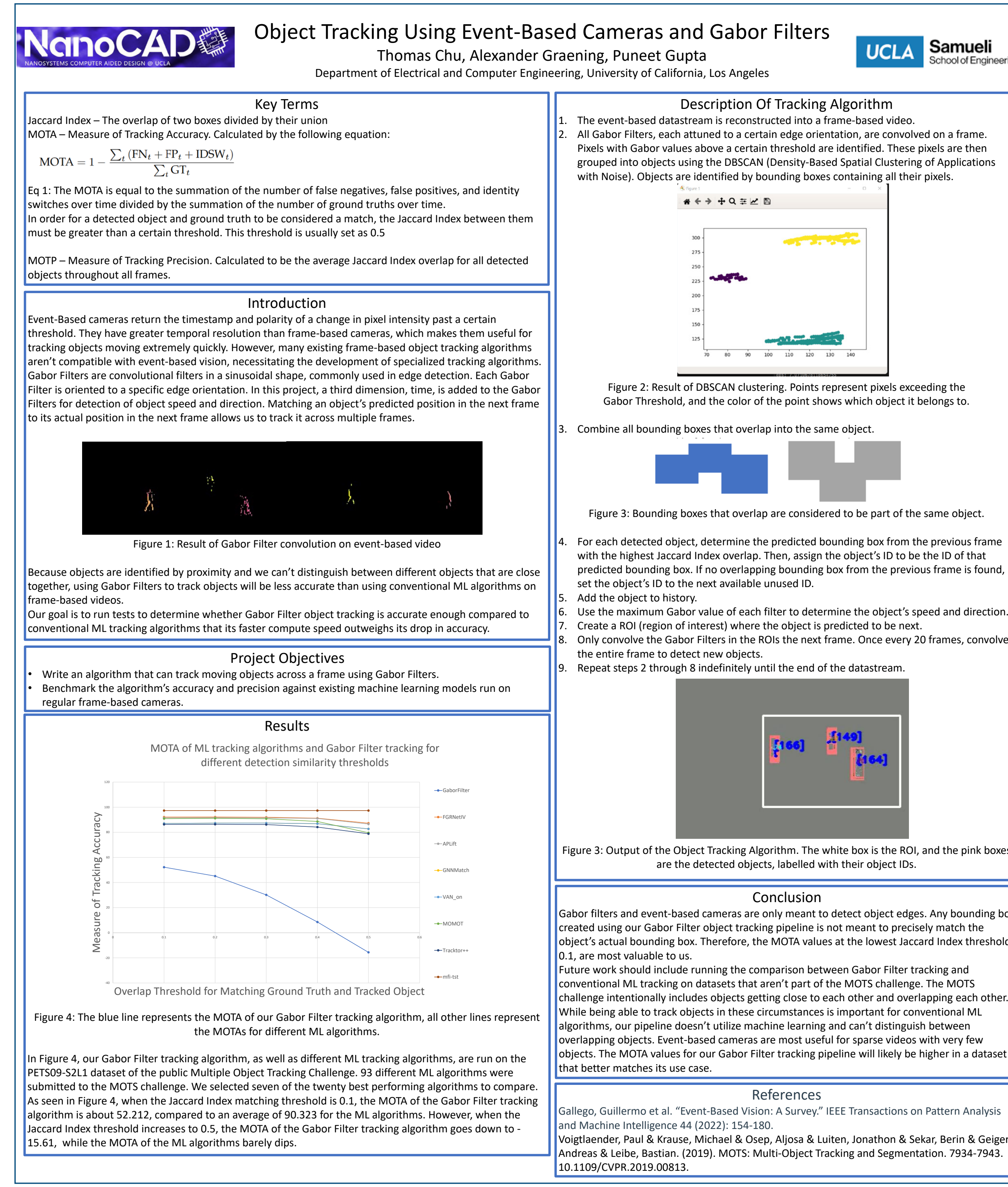

NanoCAD — NANOSYSTEMS COMPUTER AIDED DESIGN @ UCLA

Object Tracking Using Event-Based Cameras and Gabor Filters

Thomas Chu, Alexander Graening, Puneet Gupta

Department of Electrical and Computer Engineering, University of California, Los Angeles

UCLA Samueli School of Engineering

Key Terms

Jaccard Index – The overlap of two boxes divided by their union

MOTA – Measure of Tracking Accuracy. Calculated by the following equation:

$$\mathrm{MOTA} = 1 - \frac{\sum_t (\mathrm{FN}_t + \mathrm{FP}_t + \mathrm{IDSW}_t)}{\sum_t \mathrm{GT}_t}$$

Eq 1: The MOTA is equal to the summation of the number of false negatives, false positives, and identity switches over time divided by the summation of the number of ground truths over time.

In order for a detected object and ground truth to be considered a match, the Jaccard Index between them must be greater than a certain threshold. This threshold is usually set as 0.5

MOTP – Measure of Tracking Precision. Calculated to be the average Jaccard Index overlap for all detected objects throughout all frames.

Introduction

Event-Based cameras return the timestamp and polarity of a change in pixel intensity past a certain threshold. They have greater temporal resolution than frame-based cameras, which makes them useful for tracking objects moving extremely quickly. However, many existing frame-based object tracking algorithms aren't compatible with event-based vision, necessitating the development of specialized tracking algorithms. Gabor Filters are convolutional filters in a sinusoidal shape, commonly used in edge detection. Each Gabor Filter is oriented to a specific edge orientation. In this project, a third dimension, time, is added to the Gabor Filters for detection of object speed and direction. Matching an object's predicted position in the next frame to its actual position in the next frame allows us to track it across multiple frames.

Figure 1: Result of Gabor Filter convolution on event-based video

Because objects are identified by proximity and we can't distinguish between different objects that are close together, using Gabor Filters to track objects will be less accurate than using conventional ML algorithms on frame-based videos.

Our goal is to run tests to determine whether Gabor Filter object tracking is accurate enough compared to conventional ML tracking algorithms that its faster compute speed outweighs its drop in accuracy.

Project Objectives

- Write an algorithm that can track moving objects across a frame using Gabor Filters.
- Benchmark the algorithm's accuracy and precision against existing machine learning models run on regular frame-based cameras.

Results

MOTA of ML tracking algorithms and Gabor Filter tracking for different detection similarity thresholds

Measure of Tracking Accuracy

Overlap Threshold for Matching Ground Truth and Tracked Object

GaborFilter, FGRNetIV, APLift, GNNMatch, VAN_on, MOMOT, Tracktor++, mfi-tst

Figure 4: The blue line represents the MOTA of our Gabor Filter tracking algorithm, all other lines represent the MOTAs for different ML algorithms.

In Figure 4, our Gabor Filter tracking algorithm, as well as different ML tracking algorithms, are run on the PETS09-S2L1 dataset of the public Multiple Object Tracking Challenge. 93 different ML algorithms were submitted to the MOTS challenge. We selected seven of the twenty best performing algorithms to compare. As seen in Figure 4, when the Jaccard Index matching threshold is 0.1, the MOTA of the Gabor Filter tracking algorithm is about 52.212, compared to an average of 90.323 for the ML algorithms. However, when the Jaccard Index threshold increases to 0.5, the MOTA of the Gabor Filter tracking algorithm goes down to -15.61, while the MOTA of the ML algorithms barely dips.

Description Of Tracking Algorithm

1. The event-based datastream is reconstructed into a frame-based video.
2. All Gabor Filters, each attuned to a certain edge orientation, are convolved on a frame. Pixels with Gabor values above a certain threshold are identified. These pixels are then grouped into objects using the DBSCAN (Density-Based Spatial Clustering of Applications with Noise). Objects are identified by bounding boxes containing all their pixels.

Figure 2: Result of DBSCAN clustering. Points represent pixels exceeding the Gabor Threshold, and the color of the point shows which object it belongs to.

3. Combine all bounding boxes that overlap into the same object.

Figure 3: Bounding boxes that overlap are considered to be part of the same object.

4. For each detected object, determine the predicted bounding box from the previous frame with the highest Jaccard Index overlap. Then, assign the object's ID to be the ID of that predicted bounding box. If no overlapping bounding box from the previous frame is found, set the object's ID to the next available unused ID.
5. Add the object to history.
6. Use the maximum Gabor value of each filter to determine the object's speed and direction.
7. Create a ROI (region of interest) where the object is predicted to be next.
8. Only convolve the Gabor Filters in the ROIs the next frame. Once every 20 frames, convolve the entire frame to detect new objects.
9. Repeat steps 2 through 8 indefinitely until the end of the datastream.

[166] [149] [164]

Figure 3: Output of the Object Tracking Algorithm. The white box is the ROI, and the pink boxes are the detected objects, labelled with their object IDs.

Conclusion

Gabor filters and event-based cameras are only meant to detect object edges. Any bounding box created using our Gabor Filter object tracking pipeline is not meant to precisely match the object's actual bounding box. Therefore, the MOTA values at the lowest Jaccard Index threshold, 0.1, are most valuable to us.

Future work should include running the comparison between Gabor Filter tracking and conventional ML tracking on datasets that aren't part of the MOTS challenge. The MOTS challenge intentionally includes objects getting close to each other and overlapping each other. While being able to track objects in these circumstances is important for conventional ML algorithms, our pipeline doesn't utilize machine learning and can't distinguish between overlapping objects. Event-based cameras are most useful for sparse videos with very few objects. The MOTA values for our Gabor Filter tracking pipeline will likely be higher in a dataset that better matches its use case.

References

Gallego, Guillermo et al. "Event-Based Vision: A Survey." IEEE Transactions on Pattern Analysis and Machine Intelligence 44 (2022): 154-180.

Voigtlaender, Paul & Krause, Michael & Osep, Aljosa & Luiten, Jonathon & Sekar, Berin & Geiger, Andreas & Leibe, Bastian. (2019). MOTS: Multi-Object Tracking and Segmentation. 7934-7943. 10.1109/CVPR.2019.00813.

NICOLA CONTA

Electrical and Computer Engineering

1st Year, UCLA

FACULTY ADVISOR

Rob Candler

DAILY LAB SUPERVISOR

Ben Pound

DEPARTMENT

Electrical and Computer Engineering

Developing Undulators For Compact and Lower Energy Free Electron Light Sources (FEL)

ABSTRACT

Free Electron Light Sources (FEL) create intense bursts of x-rays that are millionths of a billionth of a second long, enabling unprecedented scientific discoveries: capturing the birth of chemical bonds, creating images of biological models, studying diseases, and much more. Access to FELs is limited, however, because there are few FELs in the world; current machines are very expensive (>$1B) and very long (>1km). This project aims to address both these challenges, and thus increase access, by further developing short-period undulators. The undulator is composed of alternating magnetic fields that transversely accelerate an electron beam as it travels, which generates the x-rays. Shortening the undulator period lowers the required electron beam energy to obtain a given photon wavelength, which in turn reduces the length and cost of the electron accelerator. Conventional undulators used in XFELs have period lengths around 3 cm; we designed undulators with periods of 3 and 6 mm, which would result in an accelerator length reduction of ~68%. Out of the three designs tested, simple, Halbach, and hybrid, the hybrid has the strongest field but also the highest likelihood of unacceptable field variation due to material inhomogeneities. To address this, we developed a novel method of shimming, or local magnetic field adjustment, that works within tight space constraints. Successful development of such strategies for short-period undulators has the potential to transform the field of light sources: democratizing access to discover the world on an atomic scale.

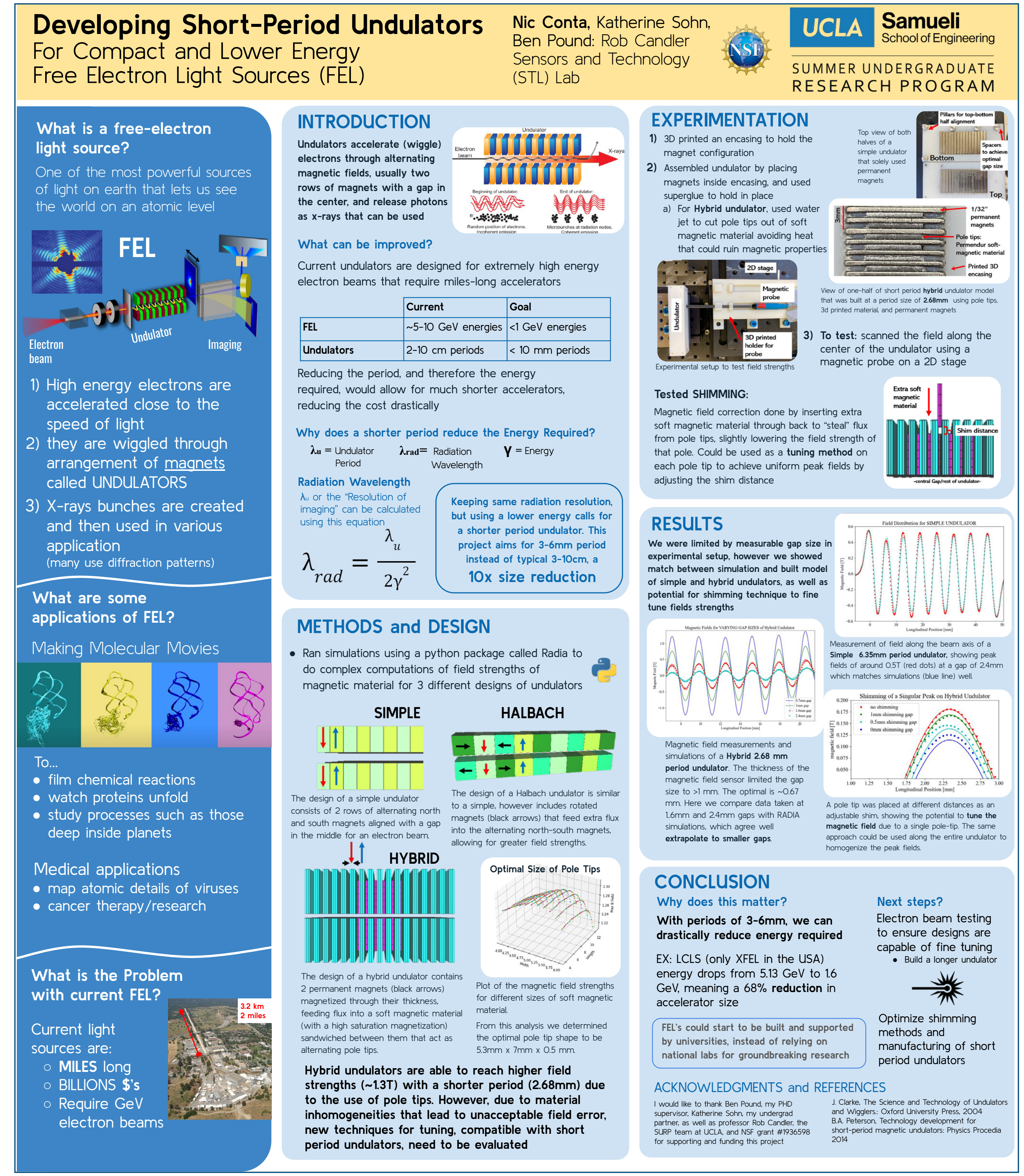

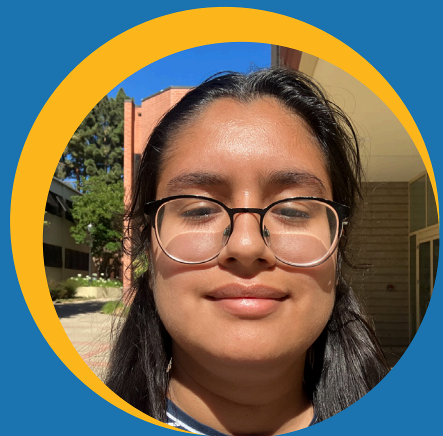

MELISSA CRUZ

Computer Science

2nd Year, El Camino College

ALEXANDER DEAL

Computer Science

1st Year, Santa Monica College

FACULTY ADVISOR

Katsushi Arisaka

DAILY LAB SUPERVISORS

Mark Diamond, Andrew Krupien

DEPARTMENT

Electrical and Computer Engineering

Stereo Depth Mapping in YOLO

ABSTRACT

While object detection algorithms are able to accurately report the positions of objects in a scene, there is no sense of 3D space. In contrast, the human brain can create a sense of depth and absolute external space automatically. Current computer vision technologies rely on complex neural networks trained on massive data sets detect objects and navigate. Images are run through hundreds of processing layers, whereas the brain has far less layers and still produces better results. Instead, humans more simply navigate by using visual displacement in their surroundings as they move their eyes and heads to create depth sensations. Our experiments take the concepts of motion parallax and the object detection algorithm, "You Only Look Once" (YOLO), to create an absolute sense of 3D space. Tests were done on various hardware: a flying drone, a quad-camera apparatus, a 2-axis laser engraver, and a dual-camera robotic car. Our findings suggest creating 3D depth sensations from displaced 2D images is possible and could greatly contribute to the advancement of current navigation systems. While our methods prove to be effective, there appears to be underlying variables such as camera technicalities. Future areas of improvement include better algorithm optimization for distant objects to improve accuracy. Additionally, we would like to integrate our technologies into a virtual reality control and feedback system, creating a more immersive experience.

Stereo Depth Mapping in YOLO

Angela Duran, Kunal Kulkarni, Melissa Cruz, Alex Deal, Mark Diamond, Andrew Krupien, Shawn Mosharaf, Katsushi Arisaka

Department of Physics and Astronomy, University of California – Los Angeles

NSF · UCLA Samueli School of Engineering · SUMMER UNDERGRADUATE RESEARCH PROGRAM

Introduction

- Modern depth perception technologies haven't fully considered humans' visual systems which have resulted in algorithms that rely on convoluted neural networks and expensive technologies such as LiDAR and Radar.
- Current research on computer-vision derives depth based on input images from a singular frame.
- This research utilizes that humans visualize objects in 2-Dimensional egocentric space relative to themselves. Furthermore, based on this visual information, the brain is able to generate its own 3-Dimensional coordinate plane based on objects' distances to each other. As such, this work seeks to implement this mechanism into stereo-depth technology.

Objective

Design a program that processes 2D images and returns the depths of recognized objects

Materials and Methods

Hardware

DJI Tello Drone, Laser Engraver, 4 x 16MP cameras attached to a raspberry Pi, Raspberry Pi controlled robotic car, You Only Look Once (YOLO) object detection software

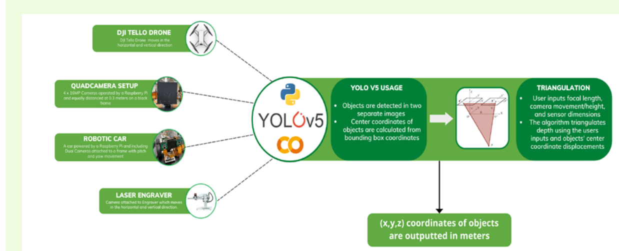

Writing the algorithm

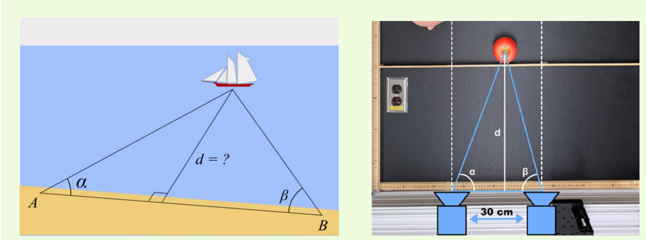

We started our research with what we knew about motion parallax. We noticed that we could integrate this concept with triangulation, a trigonometric concept that allows you to calculate the location of an object by forming triangles to the point of interest from other known points. In this case, our known points to find the location of an object would be the positions of our cameras.

Re-interpret algorithm into code

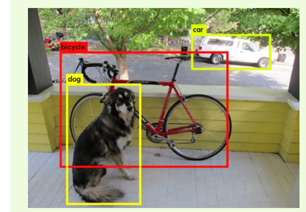

Process images using various hardware

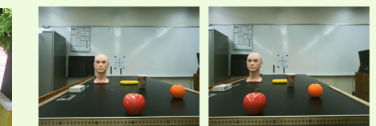

```
Enter 1 for FOV mode, Enter 2 for Ruler mode: 1
Enter Left Camera Position in m: 0.355
Enter Right Camera Position in m: 0.54
Enter Camera Height in m: 0.175
Enter Focal Length in mm: 4.04
Enter horizontal sensor length in mm: 4.71
Enter vertical sensor length in mm: 3.54
```

YOLO is an object detection algorithm capable of processing 2D egocentric images at a minimum of 45 fps. With the use of neural networks, the program finds patterns in various regions and compares that information to a database of pre trained objects. We would modify the source code to find depth, recreating 3D allocentric space.

YOLO will take in two binocular images and create bounding boxes for each frame, extracting their (x,y) pixel coordinates of each object. Using this information, the program uses triangulation to calculate the depth of objects in front of a camera. For each hardware setup, camera specs must be known to run accurate predictions.

Results

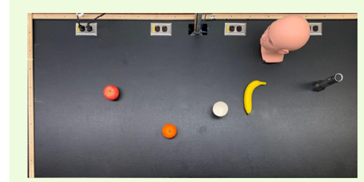

Depth Estimations in Meters

	Apple	Orange	Cup
Actual	0.45	0.77	1.20
Tello	0.51	0.85	1.69
Laser	0.57	0.88	1.31
Quadcams (Avg.)	0.53	0.75	1.08
Robot Car	0.39	0.62	0.76

The depth calculated by our algorithm is typically between 10 and 20 percent of the actual distance. With farther away objects receiving a higher error percent. The quadcams were the most accurate out of all of the used hardware and the robot car being the least accurate out of all the used hardware.

Conclusion

Though not as accurate as LiDAR, our stereo depth algorithm can be applied for a significantly cheaper price. Making it more accessible for a broader range of applications. We believe most of the error to come from pixel discrepancies with the YOLO algorithm between the two images..

References

J. Redmon, S. Divvala, R. Girshick and A. Farhadi, "You Only Look Once: Unified, Real-Time Object Detection," 2016 IEEE Conference on Computer Vision and Pattern Recognition (CVPR), 2016, pp. 779-788, doi: 10.1109/CVPR.2016.91.

Ultralytics. (n.d.). Yolov5. GitHub. https: //github.com/ultralytics/yolov5

Acknowledgements

We would like to thank the National Science Foundation for funding our project through the UCLA Summer Undergraduate Research Program. We would like to thank Professor Katsushi Arisaka for his resources, knowledge, and support. We would like to thank Will Herrera and the SURP facilitators for their guidance throughout the research process.

FACULTY ADVISOR
Jonathan Kao

DAILY LAB SUPERVISOR
Sangjoon Lee

DEPARTMENT
Electrical and Computer Engineering

VICTORIA DASILVA

Electrical and Computer Engineering

2nd Year, UCLA

Optimizing Electroencephalograph Neural Networks to Decode Human Imagination for Mind-Controlled Prosthetics

ABSTRACT

Brain-computer interfaces (BCI) enable humans to control technology, such as prosthetic limbs and computer games, with thoughts. The highest performing BCIs on the market require brain implants that read signals from hundreds of individual neurons, a surgery that can be risky and unaffordable. Electroencephalography (EEG) is a non-invasive alternative used to detect neural activity from one's scalp using a wearable cap that contains 64 electrodes. When a user imagines performing a physical movement, the electrodes record activity produced by populations of neurons firing in the sensorimotor cortex. We repeatedly trained an EEGNet convolutional neural network across multiple sessions of closed loop BCI control with the goal of producing an accurate output for a given input. To optimize this decoder, we designed and updated a game in which the cursor on a computer screen moves in a direction that corresponds to a specific thought. The user trains the cursor to move left, right, up, and down by imagining their left hand, right hand, tongue, and feet moving, respectively. To keep the cursor still, the user practices meditative rest which generates its own distinct wavelength. We hypothesize that with enough training data, the decoder will grow increasingly accurate and eventually allow for complete control of the cursor's movement on a 2-D plane. In the future, we wish to apply this neural signal processing to 3-D systems, which will allow users to have control over prostheses in a manner that is as natural as moving one's own body. Ultimately, decoding electroencephalographic data could provide the general public with access to mind-controlled technology.

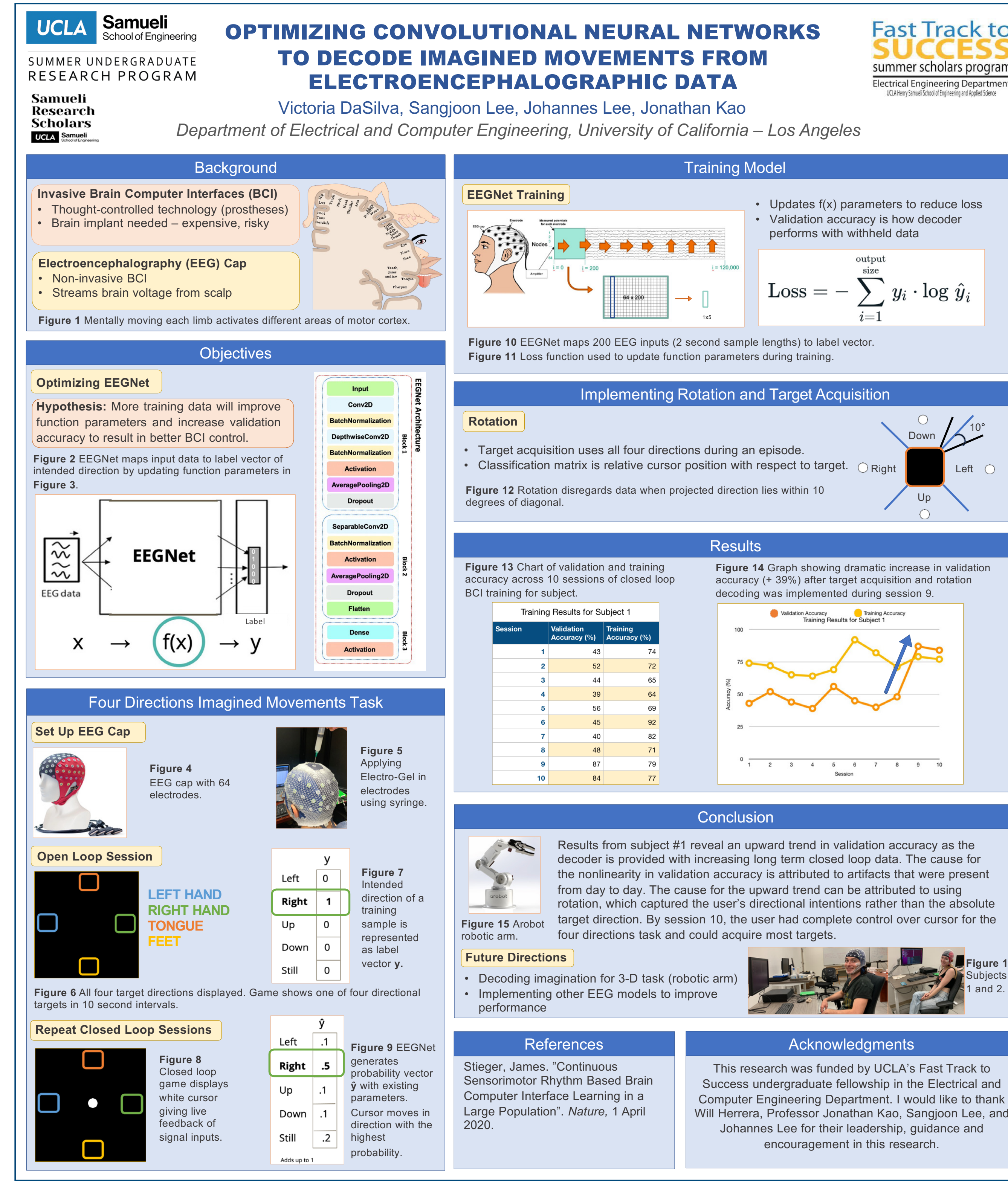

VALEN DUNN

Electrical and Computer Engineering

1st Year, UCLA

FACULTY ADVISOR

Ankur Mehta

DAILY LAB SUPERVISOR

Ankur Mehta

DEPARTMENT

Electrical and Computer Engineering

Intuitive Gestural Interfaces: Development of Intuitive input controls for complicated XR Engineering Environments.

ABSTRACT

When a designer wants to create a robot to achieve an objective, augmented reality (AR), where a user is embedded in a virtual world, has much promise due to the immersiveness of the designer computer interface and the lower overhead of computation for the creation. My research focuses on making better use of the capacity of communication from the user to the computer by interpreting more motions of the user's hands, which allows the creator to be more expressive in the scope of robot objectives. I quantified hand gestures into three vectors: the positioning of skeletal points in the hand, the rotation of the palm, and the motion of the center point of the hand. Consulting a movement expert, we were able to create a few gestures that represented the objectives of robot creation. I developed an algorithm to interpret the vectors associated with those gestures to match them to the objectives. To facilitate this match, I developed a function partitioning the vector space to map to each objective. I executed gestures multiple times with slight variations and computed the bounds of the space to create this partition. With my implementation created by refining my algorithm, an engineer with design experience within a few minutes was able to perform interpretable gestures with very little instruction. This implementation will decrease the time to learn the inputs of the augmented reality and either increase the time available to develop more robots or get a final robot out quicker.

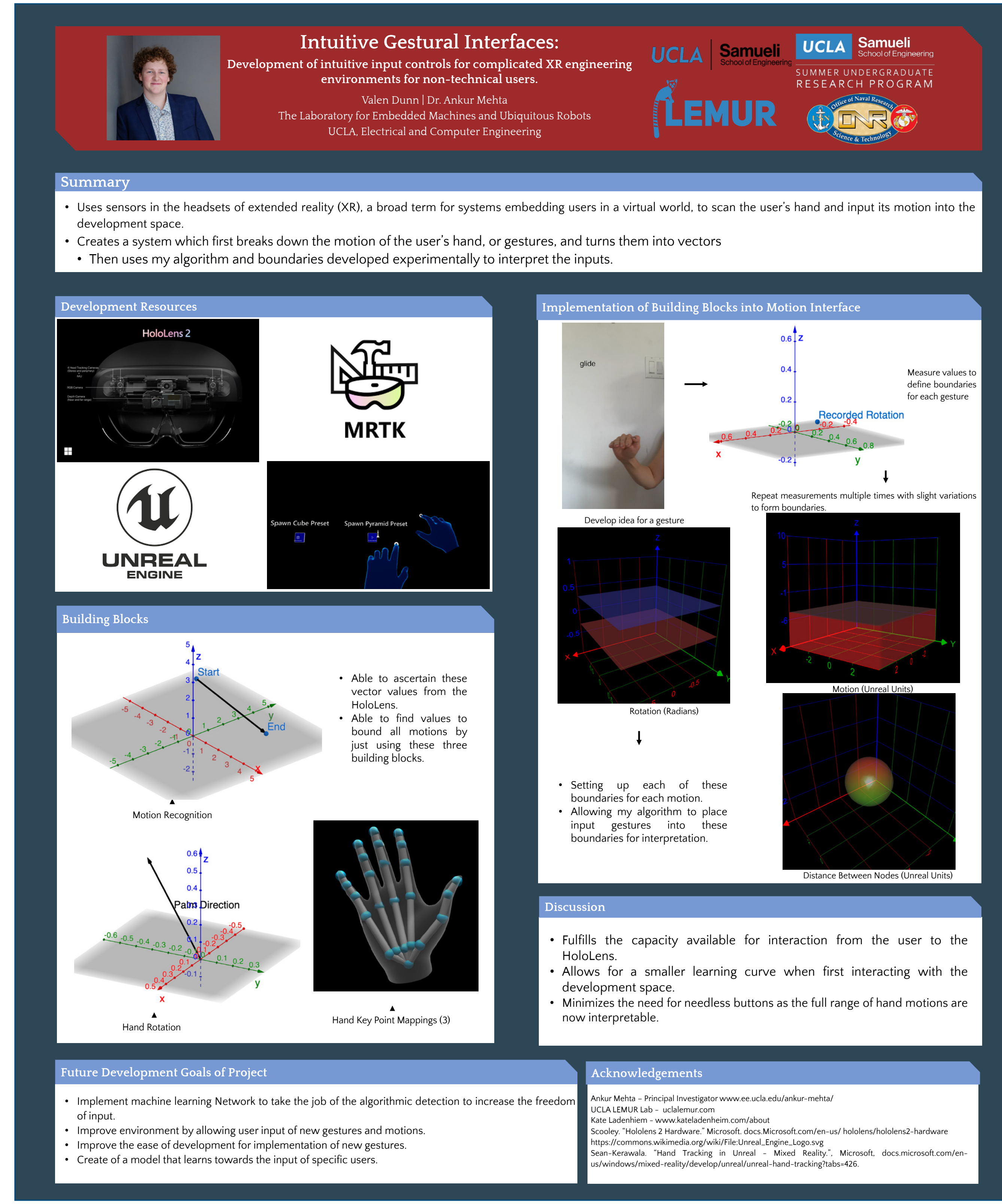

ANGELA DURAN

Computer Science
3rd Year, UCI

KUNAL KULKARNI

Computer Science/Applied Mathematics

1st Year, Irvine Valley College

FACULTY ADVISOR
Katsushi Arisaka

DAILY LAB SUPERVISORS
Mark Diamond, Andrew Krupien

DEPARTMENT
Electrical and Computer Engineering

Stereo Depth Mapping in YOLO

ABSTRACT

While object detection algorithms are able to accurately report the positions of objects in a scene, there is no sense of 3D space. In contrast, the human brain can create a sense of depth and absolute external space automatically. Current computer vision technologies rely on complex neural networks trained on massive data sets detect objects and navigate. Images are run through hundreds of processing layers, whereas the brain has far less layers and still produces better results. Instead, humans more simply navigate by using visual displacement in their surroundings as they move their eyes and heads to create depth sensations. Our experiments take the concepts of motion parallax and the object detection algorithm, “You Only Look Once” (YOLO), to create an absolute sense of 3D space. Tests were done on various hardware: a flying drone, a quad-camera apparatus, a 2-axis laser engraver, and a dual-camera robotic car. Our findings suggest creating 3D depth sensations from displaced 2D images is possible and could greatly contribute to the advancement of current navigation systems. While our methods prove to be effective, there appears to be underlying variables such as camera technicalities. Future areas of improvement include better algorithm optimization for distant objects to improve accuracy. Additionally, we would like to integrate our technologies into a virtual reality control and feedback system, creating a more immersive experience.

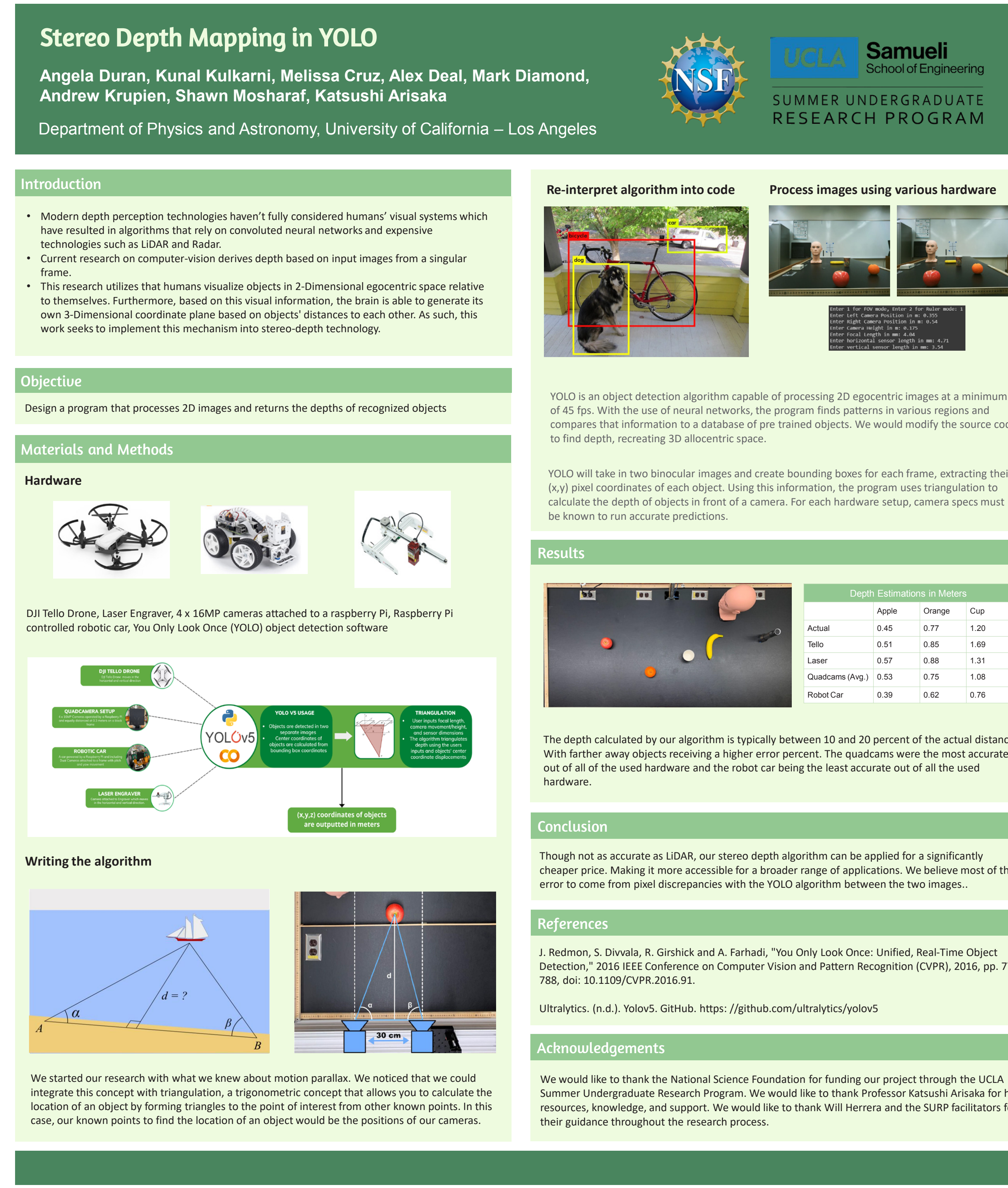

Stereo Depth Mapping in YOLO

Angela Duran, Kunal Kulkarni, Melissa Cruz, Alex Deal, Mark Diamond, Andrew Krupien, Shawn Mosharaf, Katsushi Arisaka

Department of Physics and Astronomy, University of California – Los Angeles

UCLA Samueli School of Engineering
SUMMER UNDERGRADUATE RESEARCH PROGRAM

Introduction

- Modern depth perception technologies haven’t fully considered humans’ visual systems which have resulted in algorithms that rely on convoluted neural networks and expensive technologies such as LiDAR and Radar.
- Current research on computer-vision derives depth based on input images from a singular frame.
- This research utilizes that humans visualize objects in 2-Dimensional egocentric space relative to themselves. Furthermore, based on this visual information, the brain is able to generate its own 3-Dimensional coordinate plane based on objects' distances to each other. As such, this work seeks to implement this mechanism into stereo-depth technology.

Objective

Design a program that processes 2D images and returns the depths of recognized objects

Materials and Methods

Hardware

DJI Tello Drone, Laser Engraver, 4 x 16MP cameras attached to a raspberry Pi, Raspberry Pi controlled robotic car, You Only Look Once (YOLO) object detection software

DJI TELLO DRONE
QUADCAMERA SETUP
ROBOTIC CAR
LASER ENGRAVER
YOLO V5 USAGE
- Objects are detected in two separate images
- Center coordinates of objects are calculated from bounding box coordinates

TRIANGULATION
- User inputs focal length, camera movement/height, and sensor dimensions
- The algorithm triangulates depth using the users inputs and objects' center coordinate displacements

(x,y,z) coordinates of objects are outputted in meters

Writing the algorithm

We started our research with what we knew about motion parallax. We noticed that we could integrate this concept with triangulation, a trigonometric concept that allows you to calculate the location of an object by forming triangles to the point of interest from other known points. In this case, our known points to find the location of an object would be the positions of our cameras.

Re-interpret algorithm into code

Process images using various hardware

```
Enter 1 for FOV mode, Enter 2 for Ruler mode: 1
Enter Left Camera Position in m: 0.355
Enter Right Camera Position in m: 0.54
Enter Camera Height in m: 0.175
Enter Focal Length in mm: 4.04
Enter horizontal sensor length in mm: 4.71
Enter vertical sensor length in mm: 3.54
```

YOLO is an object detection algorithm capable of processing 2D egocentric images at a minimum of 45 fps. With the use of neural networks, the program finds patterns in various regions and compares that information to a database of pre trained objects. We would modify the source code to find depth, recreating 3D allocentric space.

YOLO will take in two binocular images and create bounding boxes for each frame, extracting their (x,y) pixel coordinates of each object. Using this information, the program uses triangulation to calculate the depth of objects in front of a camera. For each hardware setup, camera specs must be known to run accurate predictions.

Results

Depth Estimations in Meters

	Apple	Orange	Cup
Actual	0.45	0.77	1.20
Tello	0.51	0.85	1.69
Laser	0.57	0.88	1.31
Quadcams (Avg.)	0.53	0.75	1.08
Robot Car	0.39	0.62	0.76

The depth calculated by our algorithm is typically between 10 and 20 percent of the actual distance. With farther away objects receiving a higher error percent. The quadcams were the most accurate out of all of the used hardware and the robot car being the least accurate out of all the used hardware.

Conclusion

Though not as accurate as LiDAR, our stereo depth algorithm can be applied for a significantly cheaper price. Making it more accessible for a broader range of applications. We believe most of the error to come from pixel discrepancies with the YOLO algorithm between the two images..

References

J. Redmon, S. Divvala, R. Girshick and A. Farhadi, "You Only Look Once: Unified, Real-Time Object Detection," 2016 IEEE Conference on Computer Vision and Pattern Recognition (CVPR), 2016, pp. 779-788, doi: 10.1109/CVPR.2016.91.

Ultralytics. (n.d.). Yolov5. GitHub. https: //github.com/ultralytics/yolov5

Acknowledgements

We would like to thank the National Science Foundation for funding our project through the UCLA Summer Undergraduate Research Program. We would like to thank Professor Katsushi Arisaka for his resources, knowledge, and support. We would like to thank Will Herrera and the SURP facilitators for their guidance throughout the research process.

FACULTY ADVISOR
Carissa Eisler

DAILY LAB SUPERVISORS
Mounika Dudala, Daniel Katz

DEPARTMENT
Chemical and Biomolecular Engineering

LEONNA GAITHER

Chemical and Biomolecular Engineering

2nd Year, UCLA

Self Assembly of Perovskite Nanocrystals

ABSTRACT

With climate change on the rise and only so limited time to save the earth, sustainability is at the forefront of issues that we need to solve. A viable solution is converting to renewable energy especially solar power, however our current technology has many limitations that make it hard to harness these natural resources. Luminescent solar concentrators are one such device which concentrate sunlight and direct it to the solar cells. Though this technology has been around for a long time, LSC's are inefficient because a significant amount of sunlight is lost due to isotropic light emissions from the LSC's. Hence having anisotropic light emission from the solar concentrator plays a major role in determining the effectiveness of the LSC's and solar cells. This project proposes an idea of orienting light emission (anisotropic) from the LSC's by forming self-assembled 2-D and 1-D perovskites lattices. This was achieved by non dimensionalizing the formed 3-D perovskite nanocubes to 2-D nano wires or 1-D nanowires (shrinking the dimensionality of the structures would lead to less scattering of the sunlight) through solvent dependent interactions of surface passivating ligands and manipulating environmental conditions such as temperature. Self-assembled superlattices perovskite structures lead to uniform monodisperse layers and optically stable nanocrystals which is required for large scale applications.

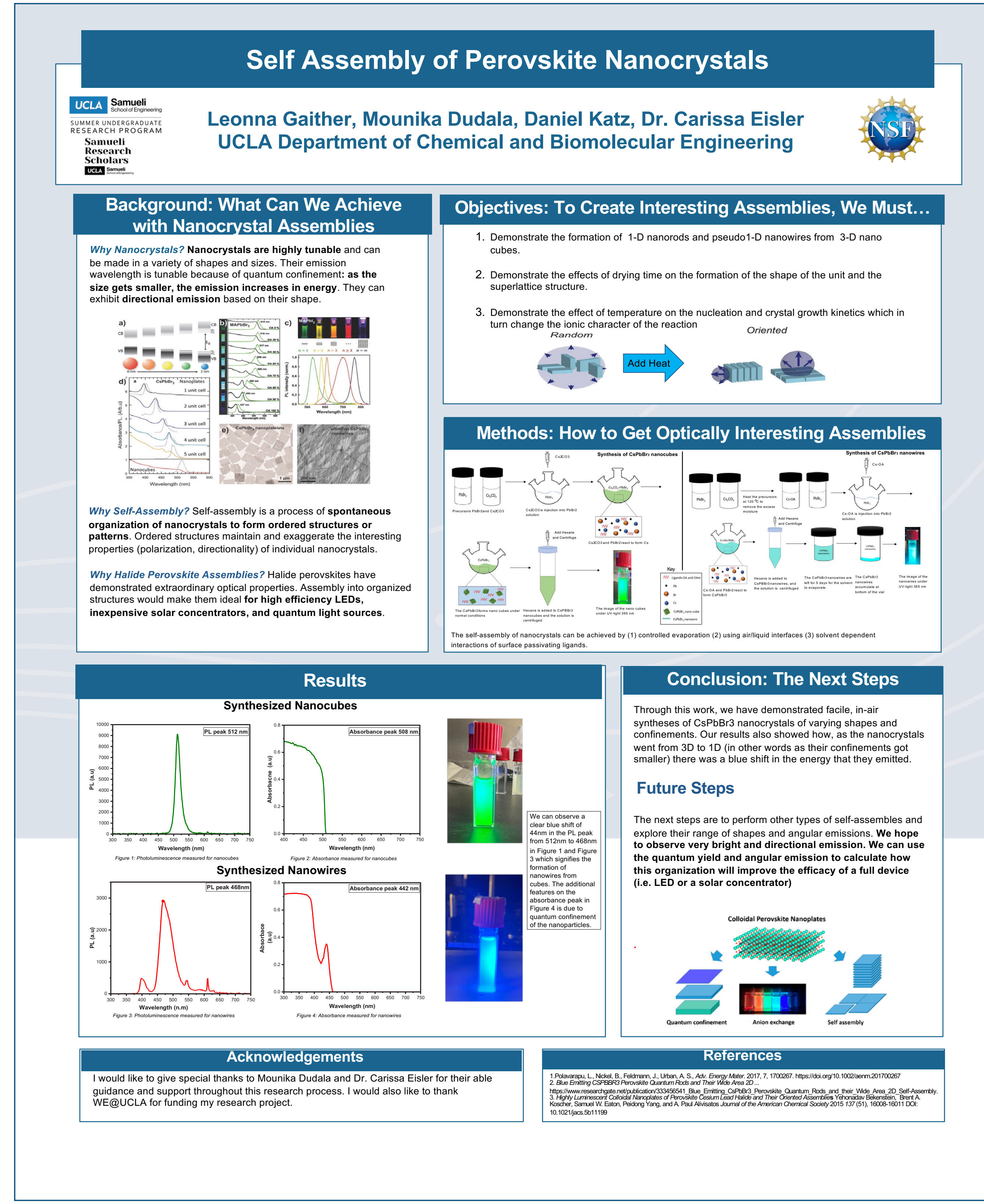

FACULTY ADVISOR

Richard Wesel

DAILY LAB SUPERVISORS

Jacob King, Hengjie Yang

DEPARTMENT

Electrical and Computer Engineering

HOLDEN GRISSETT

Computer Science and Engineering

3rd Year, UCLA

Designing High-Rank Distance-Spectrum-Optimal CRC polynomials for High-Rate Convolutional Codes

ABSTRACT

5G technology has been enabled by recent advances in coding theory, such as polar codes. However, many applications remain out of reach. Without sufficiently low error-rate and low latency, a class of applications, dubbed “mission-critical” applications due to their strict error and latency requirements, remain out of reach of current wireless communication technology. However, much progress has been made to close this gap. One such area, list-decoding, is a subject of research at Professor Wesel’s Communications Systems Laboratory. It has already been shown that both high-rate and low-rate zero-terminated and tail-biting convolutional codes (ZTCCs and TBCCs) with cyclic- redundancy-check (CRC)-aided list decoding techniques closely approach the random-coding union (RCU) bound for short blocklengths. However, current program implementations have limited our ability to design higher-rank CRCs in these papers. In our research, we use software engineering techniques to improve the performance of the current CRC search algorithm and mitigate an important memory-bandwidth bottleneck. We are then able to use these performance improvements to design higher-rank CRCs.

EVY HAYNES

Mechanical and Aerospace Engineering

2nd Year, UCLA

FACULTY ADVISOR

Artur Davoyan

DAILY LAB SUPERVISOR

Ho-Ting Tung

DEPARTMENT

Mechanical and Aerospace Engineering

Development of Photonics Spacecraft Propulsion using Novel Materials and Nanophotonic Designs

ABSTRACT

New methods of spacecraft propulsion have been continuously studied since the emergence of astronautics in order to make space travel cheaper and faster, while still collecting data that teaches us more about the universe. Solar sails utilize the momentum of reflected photons to accelerate low mass spacecraft to unprecedented speeds without needing to carry onboard fuel, meaning that they are not limited by the rocket equation as compared to a chemically or electrically propelled vehicle. If successful, a vehicle powered by a solar sail would accelerate near the sun and be able to fly at solar latitudes outside the ecliptic plane and obtain new information about the Sun. To effectively accelerate, it must be ultra lightweight and reflect as much light as possible, it should also be made of a material that withstands extreme temperatures close to the sun while passively cooling the spacecraft and that which it carries. This requires a low density material with a low solar absorptivity and high thermal emissivity. Coating an ultrathin metal such as titanium nitride with an inorganic substrate such as carbon or boron nitride nanotube combines the strength and reflectivity of the metal with the thermal emissivity of the substrate, allowing for a material that could make up a functional solar sail. Here I will overview our work on design and fabrication of such thin films. I will show that ~1 micron thick films can be fabricated by solution process methods and transferred onto various substrates for subsequent post processing.

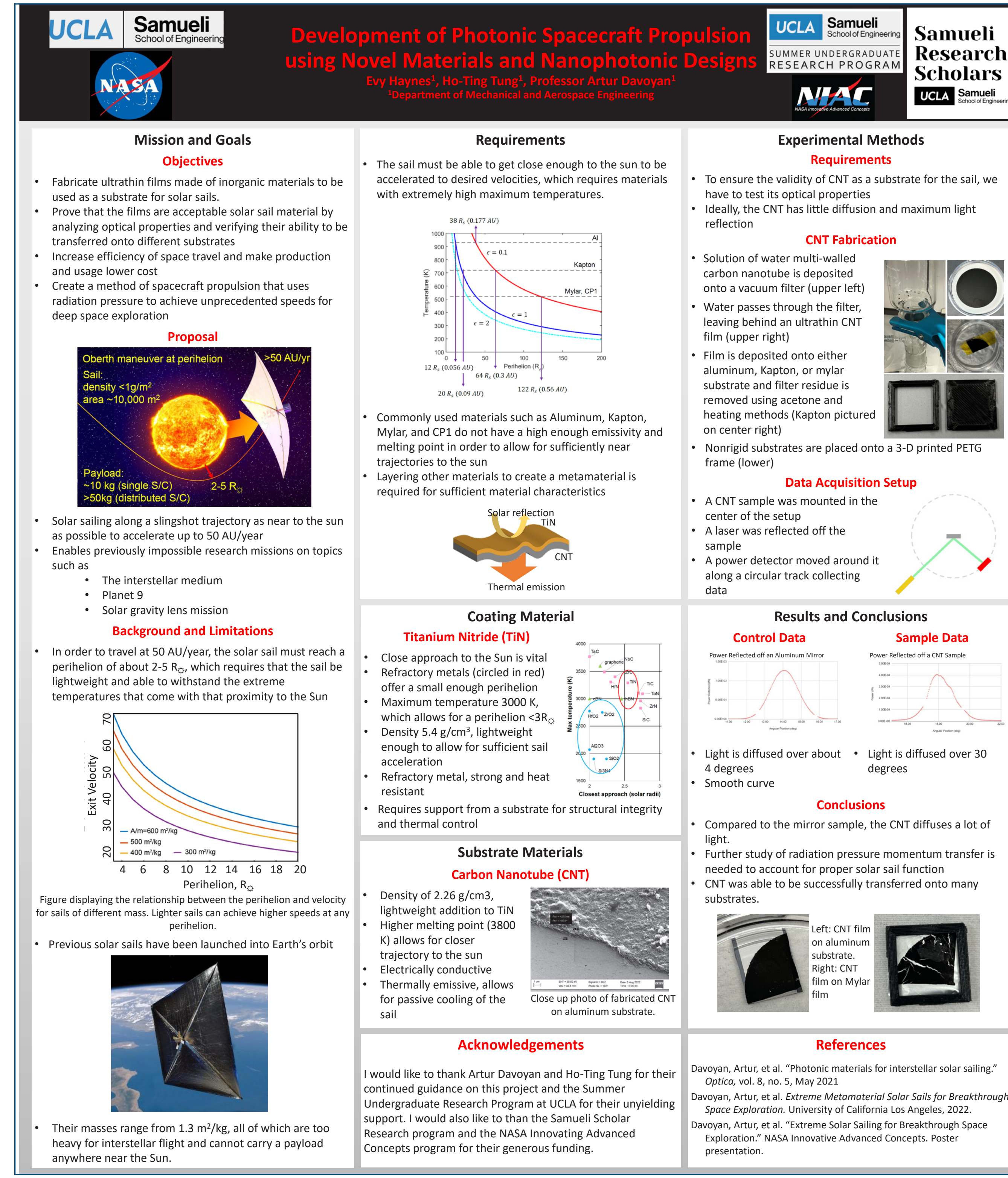

FACULTY ADVISOR
Lihua Jin

DAILY LAB SUPERVISOR
Chen Wei

DEPARTMENT
Mechanical and Aerospace Engineering

BENNY HSU

Mechanical and Aerospace Engineering

2nd Year, UCLA

Fracture Mechanics of Liquid Crystal Elastomers

ABSTRACT

Liquid Crystal Elastomers (LCEs) are a unique type of soft material combining flexible polymer network and rod-like liquid crystals (LCs) that can withstand higher strain than classical elastomers due to the reorientation of LCs. With more applications of LCEs starting to be realized, it will be crucial to understand the fracture mechanics of LCEs so future engineers would be able to prevent possible failures. The purpose of this research is to understand the fracture mechanics of LCEs by investigating the strain and displacement fields and the director rotation around a crack tip. To achieve strain and displacement measurements, we fabricated main-chain monodomain LCEs films with a small edge-crack, and stretched parallel, perpendicular and oblique to the initial director with different angles. The Digital Image Correlation (DIC) method through the Ncorr program on MATLAB was utilized to track the displacement and strain distribution in the LCE samples. The rotation of the director was measured using the optical polariscope method. In general, we found the directors around the crack tip field rotate to be tangential to the crack surface, and the directors at remote regions realigned to the stretching direction. The overall strain and displacement fields match with the simulation where displacement concentration around the crack tip shifts for the specimens with different initial directors. Future work on fatigue cycle and internal imperfection of LCEs would have to be done to understand the fracture mechanics of LCE thoroughly.

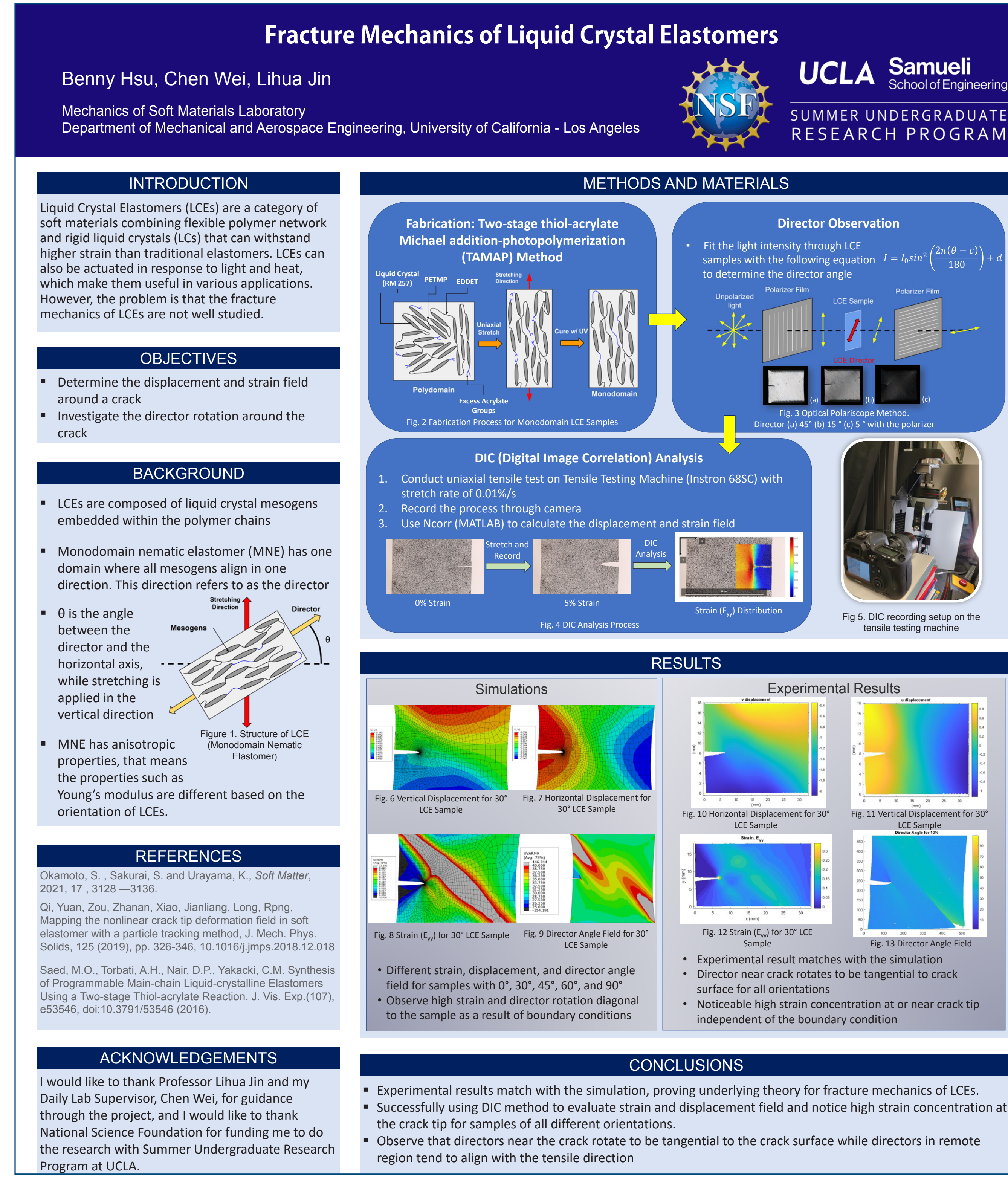

MAI LYNN HUNT

Electrical Engineering

2nd Year, Hartnell Community College

FACULTY ADVISOR
Ankur Mehta

DAILY LAB SUPERVISOR
Ankur Mehta

DEPARTMENT
Electrical and Computer Engineering

Design of Bio-Inspired Cut-and-Fold Robot Bodies

ABSTRACT

We live in an era of technology and innovation where robots are taking inspiration from nature in order to solve complex problems. However, not everyone has access to these advancements due to the complexity of robot design and manufacturing. By introducing an inexpensive, streamlined, and simplified approach– cut-and-fold robots– we aim to increase the accessibility of bio-inspired robot creation. Our objective is to diversify the functionality of cut-and-fold robots by translating the natural ability of a three banded armadillo to enclose itself. I adapted a two-dimensional cut-and-fold template for an armadillo, which I then sent to a desktop paper cutter to ensure precise fabrication. Prototypes were fabricated using cardstock and thin plastic sheets since they are relatively inexpensive, easily deformable materials. I found that the cardstock better mimicked the rolling motion of an armadillo; the plastic sheets were too rigid. We wanted an easy way to roll and unroll the body, so we implemented a string system by sewing fishing line into its sides. When pulling the fishing line, we could transition the armadillo between its rolled and unrolled state. For future works we would like to explore additional bio-inspired mechanisms. Adapting bio-inspired designs to the cut-and-fold context will aid in making a larger variety of robotic functions more accessible to a general audience.

MATHEO IRAZABAL

Electrical and Computer Engineering

1st Year, UCLA

FACULTY ADVISOR

Clarice Aiello

DAILY LAB SUPERVISOR

Andrei Tretiakov

DEPARTMENT

Electrical and Computer Engineering

Biological Effects of Moderate Static Magnetic Fields

ABSTRACT

Evidence spanning decades indicates that weak magnetic fields affect various types of organisms in many different ways. For example, this is seen in animals that display magnetoreception, which is the ability to detect the Earth's magnetic field navigation during migration season. However, more research is needed to determine how magnetic fields interact with or affect smaller organisms at the cellular level. We seek to determine how weak magnetic fields are altering the physiology of organisms. We also aim to systematize and corroborate or refute the evidence found in previously published experiments. Towards that goal, we are first constructing our own 3-Axes Helmholtz Coils to have greater control over the way the magnetic field interacts with a given cell culture. After building the coils, we will test their efficiency, making sure they perform relatively close to our simulations. Finally, the instrument will be placed inside an incubator. Up to 4 standard 12-well cell culture plates will be hosted within the Helmholtz Coils, and we will observe any changes on them as a function of DC magnetic field strength and exposure times. Preliminary results done with a one-directional Helmholtz coil on Actin, Tubulin, and Mitochondria within smooth muscle cells for 4 hours with a magnetic field of 6 mT show some deformation of mitochondrial and actin structures.

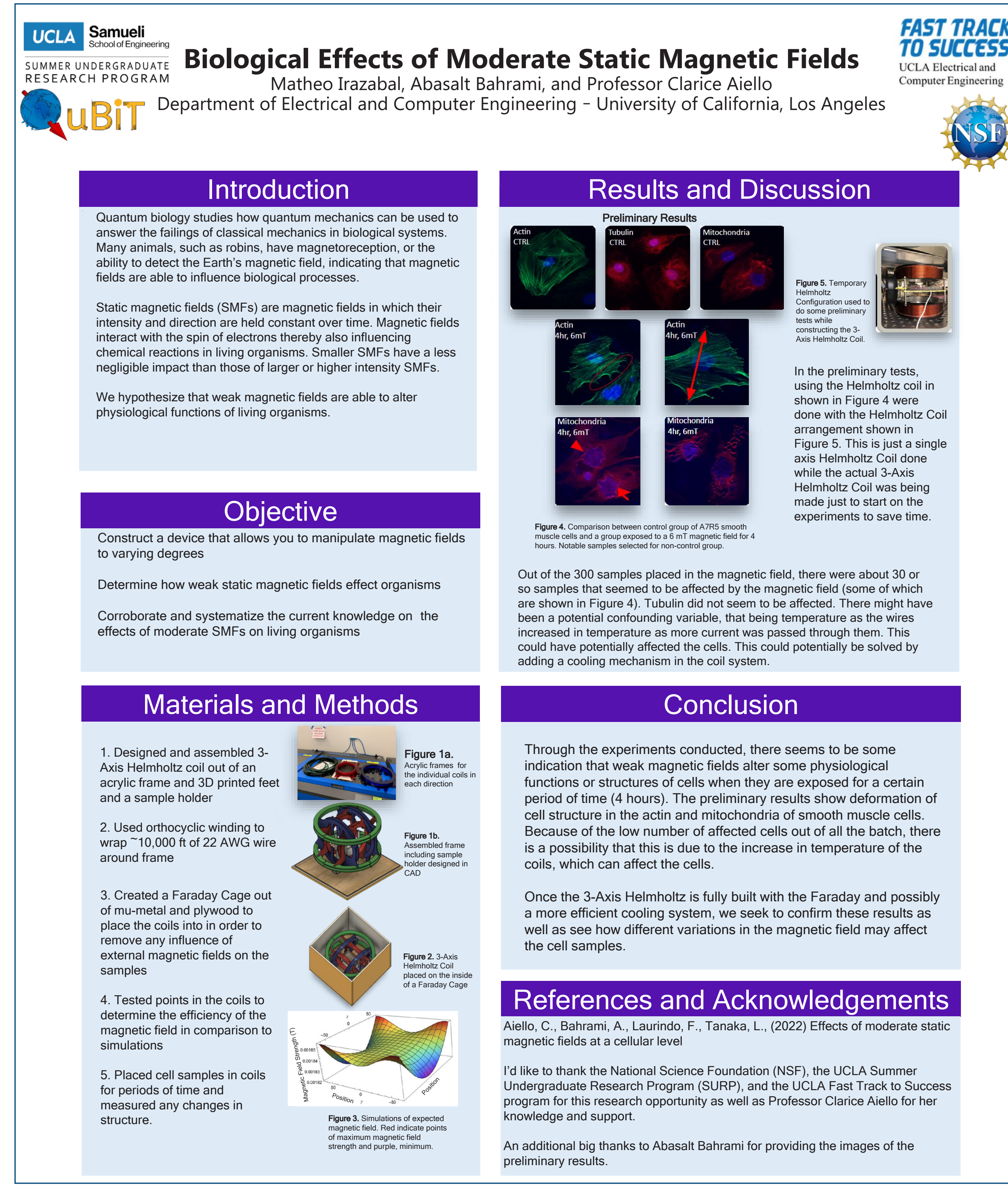

UCLA Samueli School of Engineering
SUMMER UNDERGRADUATE RESEARCH PROGRAM
QuBiT

FAST TRACK TO SUCCESS
UCLA Electrical and Computer Engineering

NSF

Biological Effects of Moderate Static Magnetic Fields

Matheo Irazabal, Abasalt Bahrami, and Professor Clarice Aiello
Department of Electrical and Computer Engineering – University of California, Los Angeles

Introduction

Quantum biology studies how quantum mechanics can be used to answer the failings of classical mechanics in biological systems. Many animals, such as robins, have magnetoreception, or the ability to detect the Earth's magnetic field, indicating that magnetic fields are able to influence biological processes.

Static magnetic fields (SMFs) are magnetic fields in which their intensity and direction are held constant over time. Magnetic fields interact with the spin of electrons thereby also influencing chemical reactions in living organisms. Smaller SMFs have a less negligible impact than those of larger or higher intensity SMFs.

We hypothesize that weak magnetic fields are able to alter physiological functions of living organisms.

Objective

Construct a device that allows you to manipulate magnetic fields to varying degrees

Determine how weak static magnetic fields effect organisms

Corroborate and systematize the current knowledge on the effects of moderate SMFs on living organisms

Materials and Methods

1. Designed and assembled 3-Axis Helmholtz coil out of an acrylic frame and 3D printed feet and a sample holder

2. Used orthocyclic winding to wrap ~10,000 ft of 22 AWG wire around frame

3. Created a Faraday Cage out of mu-metal and plywood to place the coils into in order to remove any influence of external magnetic fields on the samples

4. Tested points in the coils to determine the efficiency of the magnetic field in comparison to simulations

5. Placed cell samples in coils for periods of time and measured any changes in structure.

Figure 1a. Acrylic frames for the individual coils in each direction

Figure 1b. Assembled frame including sample holder designed in CAD

Figure 2. 3-Axis Helmholtz Coil placed on the inside of a Faraday Cage

Figure 3. Simulations of expected magnetic field. Red indicate points of maximum magnetic field strength and purple, minimum.

Results and Discussion

Preliminary Results

Figure 4. Comparison between control group of A7R5 smooth muscle cells and a group exposed to a 6 mT magnetic field for 4 hours. Notable samples selected for non-control group.

Figure 5. Temporary Helmholtz Configuration used to do some preliminary tests while constructing the 3-Axis Helmholtz Coil.

In the preliminary tests, using the Helmholtz coil in shown in Figure 4 were done with the Helmholtz Coil arrangement shown in Figure 5. This is just a single axis Helmholtz Coil done while the actual 3-Axis Helmholtz Coil was being made just to start on the experiments to save time.

Out of the 300 samples placed in the magnetic field, there were about 30 or so samples that seemed to be affected by the magnetic field (some of which are shown in Figure 4). Tubulin did not seem to be affected. There might have been a potential confounding variable, that being temperature as the wires increased in temperature as more current was passed through them. This could have potentially affected the cells. This could potentially be solved by adding a cooling mechanism in the coil system.

Conclusion

Through the experiments conducted, there seems to be some indication that weak magnetic fields alter some physiological functions or structures of cells when they are exposed for a certain period of time (4 hours). The preliminary results show deformation of cell structure in the actin and mitochondria of smooth muscle cells. Because of the low number of affected cells out of all the batch, there is a possibility that this is due to the increase in temperature of the coils, which can affect the cells.

Once the 3-Axis Helmholtz is fully built with the Faraday and possibly a more efficient cooling system, we seek to confirm these results as well as see how different variations in the magnetic field may affect the cell samples.

References and Acknowledgements

Aiello, C., Bahrami, A., Laurindo, F., Tanaka, L., (2022) Effects of moderate static magnetic fields at a cellular level

I'd like to thank the National Science Foundation (NSF), the UCLA Summer Undergraduate Research Program (SURP), and the UCLA Fast Track to Success program for this research opportunity as well as Professor Clarice Aiello for her knowledge and support.

An additional big thanks to Abasalt Bahrami for providing the images of the preliminary results.

FACULTY ADVISOR
Nader Sehatbakhsh

DAILY LAB SUPERVISOR
Justin Feng

DEPARTMENT
Electrical and Computer Engineering

TIMOTHY JACQUES

Electrical and Computer Engineering

2nd Year, UCLA

Identification of Embedded Devices via Electromagnetic Emissions

ABSTRACT

Securely identifying an electronic device can be extremely difficult. The majority of current solutions, such as RFIDs or printed barcodes are either too expensive to realistically use at industrial scale, or too easy to spoof and therefore insecure. Due to these limitations, finding an alternative that fulfills both criteria is highly desired. Electromagnetic emissions have been proven to be unique enough to identify individual devices from one another, and add no extra cost to device manufacturing. However, it has yet to be shown that it is possible to identify devices at extended ranges, especially when such devices do not have wireless transceivers. We show that by analyzing the emanations for common features across device types while still retaining individuality, it is still possible to recover enough data at range (>1 meter) to uniquely identify separate devices. Electromagnetic emissions from several development boards in various states (idle, running a simple program) were obtained using a USRP Software-Defined Radio and GNURadio. This data was then processed in MATLAB to first extract useful features that are both unique to individual devices and consistent over time, for usage in feature based classification models. The extracted features were then supplied to a Random Forest classifier to identify specific devices. Initial results from the model show that it is possible to identify devices at 1 meter of range with a success rate of 91%. Therefore, our feature-based machine learning model is able to determine not only the type of the device in range but also the exact individual device, demonstrating the feasibility of this method for secure identifcation.

STEVE LEE

Computer Engineering

1st Year, UCLA

FACULTY ADVISOR

Puneet Gupta

DAILY LAB SUPERVISOR

Shurui Li

DEPARTMENT

Electrical and Computer Engineering

Compression of Convolutional Neural Networks on One-Dimensional Datasets via Weight Pool Networks

ABSTRACT

Convolutional neural networks are often used in a variety of classification and prediction models, most commonly in the field of image processing. However, as some of these neural networks become increasingly deep and complex, their requisite computational power and storage size may start to look unviable for resource-constrained devices. Compression techniques such as weight pooling serve to cluster neural network weights together and reduce the number of weights needed to be stored. We specifically used channel-wise weight pooling to allow for groupings on arbitrary 2D filter sizes while minimizing accuracy drop. As this approach has exhibited an adequately low drop in accuracy when run on an image dataset, we applied the same methods to one-dimensional datasets such as Deepsig's RadioML dataset. Generating weight pools of size 64 allows for 7.6x compression while showing similar levels of accuracy compared to the original network.

Compression of Convolutional Neural Networks on One-Dimensional Datasets via Weight Pool Networks

UCLA Samueli School of Engineering

Steve Lee, Shurui Li, Puneet Gupta

Department of Electrical and Computer Engineering, University of California, Los Angeles

UCLA Samueli School of Engineering SUMMER UNDERGRADUATE RESEARCH PROGRAM

Introduction

- Objectives
  - Many neural networks nowadays too advanced for deployment on resource-constrained devices
  - We seek to achieve optimal compression of NNs with minimal accuracy drop in order to reduce requisite computing power or memory
  - We would like to evaluate the efficacy of weight pool networks along the z-axis dimension (channel-wise pooling) on datasets other than images
- Background
  - Convolution involves altering each element of a matrix by combining information from its surrounding elements and a particular filter
  - Pooling is the process of directly compressing a matrix down by aggregating data into clusters and extracting a single value from each cluster
  - Convolutional Neural Networks (CNN) use a combination of convolution and pooling layers to compress the input layer down to a much smaller size
  - Instead of pooling on a two-dimensional scale, we cluster weights on a channel-wise basis to allow for arbitrary filter size

Figure [1]: Sample schematic of a convolutional neural network. Input is run through several convolutional layers before any activation functions in the hidden layers

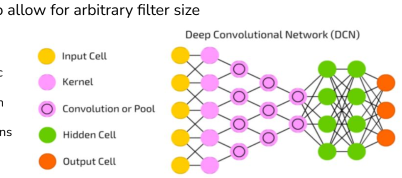

Materials and Methods

- Materials
  - PyTorch: Machine learning framework allowing for operations on weights with parallelism
  - Deepsig RadioML 2016.10A Dataset: Synthesized RF dataset with pre-classified modulations
  - Speech Commands audio dataset

DEEPSIG

- Methodology
  - Conducted training on Deepsig RadioML dataset using two convolutional layers (1x3 and 2x3 filter, respectively) and Adam optimization algorithm
  - Conducted training on Speech Commands dataset using 4 convolutional layers
  - Trained using 256 samples per batch
  - By stacking filters and pooling weights along the channel-dimension, we can represent each weight with an index to the weight pool's center instead
  - After 8-bit channel-wise pooling using K-means clustering algorithm, there will be 32, 64, 128, or 256 groups of vectors
  - Retrained original neural network while integrating weight pool clusters to regenerate a compressed neural network
  - RF dataset can be treated as a very long two-dimensional dataset due to separated IQ components

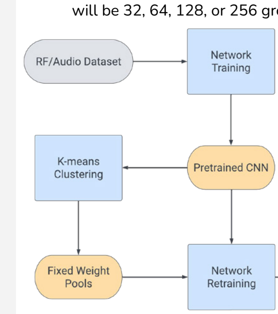

Figure [2]: Flow of methodology; original neural network trains on the dataset and generates weight pools using K-means clustering. Afterwards, the pre-trained weights and weight pools are used to retrain a new, compressed network

Results

- All neural networks were trained until average classification accuracy converged (between 100 and 200 epochs)
- Accuracy on both datasets converge at around 80%, and remains roughly the same after compression
- Neural network on audio dataset was trained using varying sizes of weight pool networks (ranging between 32 and 256 groups)
- Neural network on RF dataset was trained only using weight pool size of 64
- Increasing size of weight pools would theoretically increase accuracy, but lead to issues when measuring speedup later on
- RF dataset consists of subsets of varying signal-to-noise ratios; modulation classification accuracy should be higher for stronger relative signal strength
- Weight pooling was excluded on the first layers of both networks, so the compression factor for the RF dataset is 7.7x (two layers) while the compression factor for the audio dataset is 4.6x (four layers)

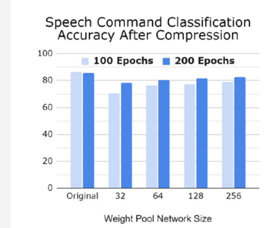

Figure [3]: Audio neural network accuracy according to varying weight pool sizes

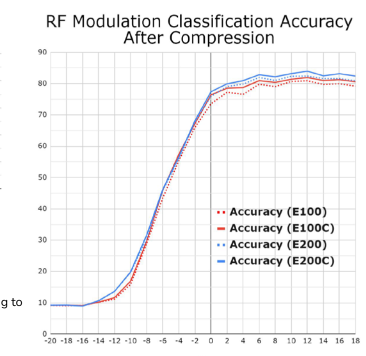

Figure [4]: Radio frequency signal neural network accuracy according to varying SNRs

Conclusions

- Classification accuracy drop for RF dataset is negligible after compression and increases in some cases (since network was trained for 200 epochs both before and after compression)
- Accuracy drop in speech command classification is larger but still insignificant especially when trained with weight pool size of 256 clusters
- Results show that weight pooling allowed for compression of convolutional neural networks with satisfactory accuracy retention
- Future progress can be found in combining channel-wise weight pooling with other compression techniques to improve accuracy or increase compression

References

- Li, S., & Gupta, P. (2022). Bit-serial Weight Pools: Compression and Arbitrary Precision Execution of Neural Networks on Resource Constrained Processors. doi:10.48550/ARXIV.2201.11651
- O'Shea, T. J., Corgan, J., & Clancy, T. C. (2016). Convolutional Radio Modulation Recognition Networks. doi:10.48550/ARXIV.1602.04105
- Van Veen, Fjodor (2016). A mostly complete chart of Neural Networks. asimovinstitute.org

Acknowledgements

I would like to thank Professor Puneet Gupta for allowing me to work in his lab as well as Shurui Li for mentoring and guiding me through this project. I would also like to thank the Interactive Systems REU site for funding this project.

FACULTY ADVISORS

Chandra Joshi, Sergei Tochitsky

DAILY LAB SUPERVISOR

Daniel Matteo

DEPARTMENT

Electrical and Computer Engineering

LANA LIM

Electrical and Computer Engineering

1st Year, UCLA

Automation of High-repetition Rate Spectral Measurement for Use in Research of Infrared Supercontinuum Generation

ABSTRACT

Optics research and applications often require accurate and precise measurements of the power, time-of-flight, or spectral content of a laser. Examples of this include lidar, spectroscopy or supercontinuum (SC) generation, a nonlinear optical process in which a short pulse laser experiences extreme spectral broadening after passing through a material. Current data acquisition systems for spectral measurements operate at an acquisition rate of around 1 Hz using a monochromator, photodetector, and oscilloscope. High speed data acquisition systems must be implemented to accurately measure the spectral content of lasers operating at a repetition rate of 1 kHz. We created a mock-up experimental setup with a variable pulse length 656.6 nm diode laser to focus on automating the spectral data collection process. Communication with the oscilloscope and monochromator was accomplished by Python code. We produced an acquisition rate of around 50 Hz, the maximum frequency before the oscilloscope collected repeated values. We tested the data acquisition framework by first mapping the spectrum of the diode laser to determine its central wavelength and bandwidth. Then, we measured spectra consisting of multiple diffraction orders over a wide range of grating angles. Future steps will focus on implementing the automated data collection process in experiments in the mid-infrared spectral range.

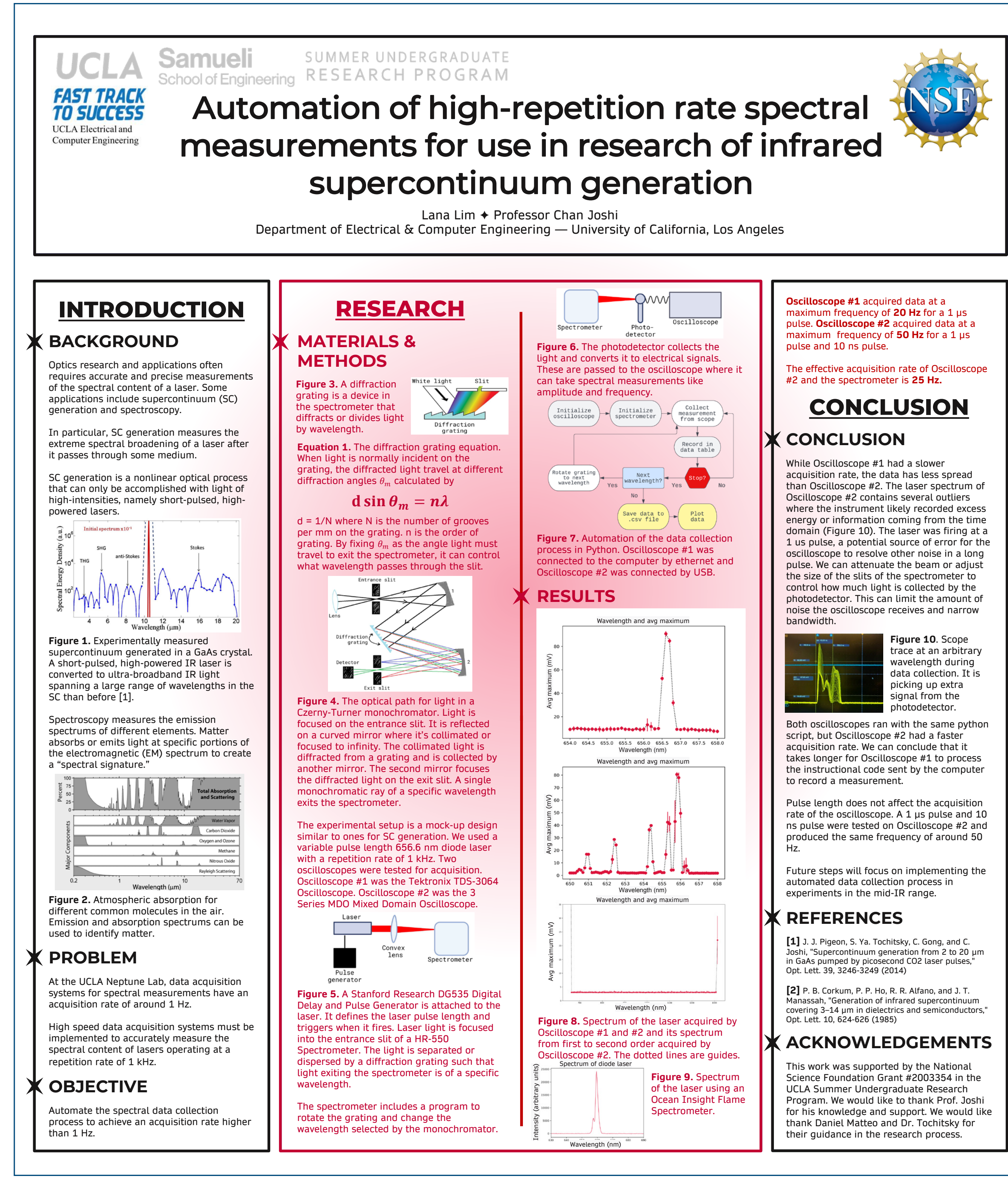

RANDY LIU

Electrical and Computer Engineering

1st Year, UCLA

FACULTY ADVISOR

Jason Speyer

DAILY LAB SUPERVISOR

Nat Snyder

DEPARTMENT

Mechanical and Aerospace Engineering

Windowed Cauchy Estimation for Multi-State Systems

ABSTRACT

Bayesian state estimators use both noisy measurement data and prior knowledge about the stochastic dynamics of a system to make an inference about the true value of the state. Since 1960, only one estimation scheme in which the dynamic generation of the conditional probability density function given the measurement history is recursive and analytic - the celebrated Kalman filter. A Kalman filter applies Bayesian estimation for linear dynamics over discrete time steps to estimate a state over time. However, the Kalman filter assumes the state to be a normal (Gaussian) distribution, a light tailed distribution, and thus is inadequate for systems with heavy-tailed noise, or those with higher probability of data distributed towards the tails of the probability density function. Thus, the analytic and recursive Cauchy estimator was developed basing the (modeled) process and measurement noises on the heavy-tailed Cauchy distribution. Because the amount of memory and computation required for the Cauchy estimator grows indefinitely with each discrete time step, a sliding window approximation was implemented to ensure an estimator with a fixed amount of computation and memory could be made at any given time step. This windowed Cauchy algorithm was tested on a nonlinear three-state model of a homing missile with radar measurement. When the algorithm was used to estimate the position, relative velocity, and target acceleration of the missile over time, it was found to significantly outperform the Kalman filter, even with smaller window sizes. Because larger window sizes require more computation and memory, different window sizes were tested against each other. Little significant decrease in estimation accuracy was measured at smaller window sizes, thus implying that the windowed Cauchy filter can practically be applied without excessive computational power. Future research will include testing the Cauchy estimator on different applications which are found to have heavy-tailed noise.

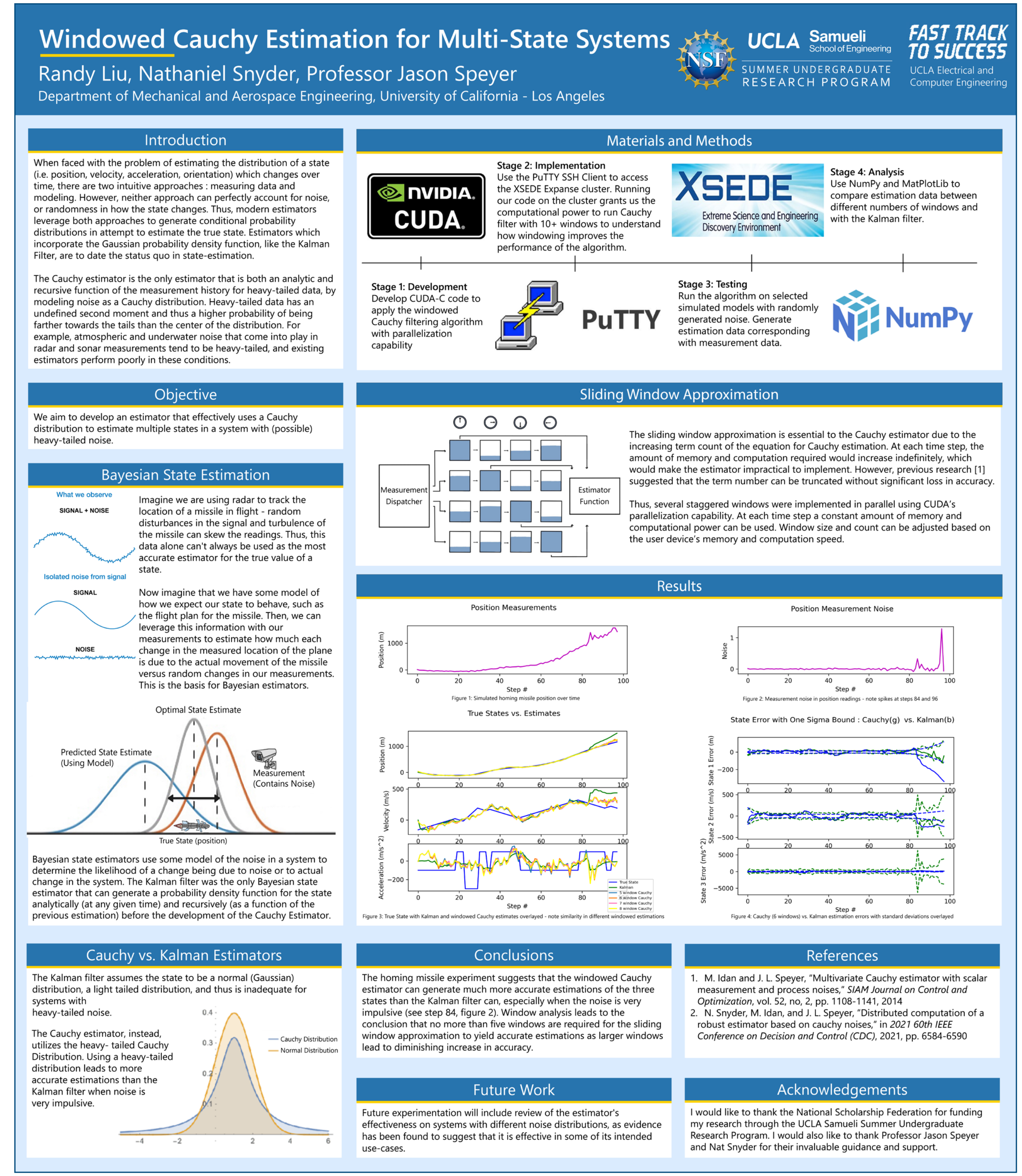

BILAL MALIK

Computer Science

1st Year, El Camino College

FACULTY ADVISOR
Ankur Mehta

DAILY LAB SUPERVISOR
Ankur Mehta

DEPARTMENT
Electrical and Computer Engineering

Intuitive Environmental Design in Virtual Reality for Robotic Simulation

ABSTRACT

The field of robotics needs simpler tools to create robots, especially for nonexperts, as the complete process is tedious and not user-friendly. A part of testing a robot is evaluating how it will physically interact with an environment through handling an obstacle or traversing certain terrain. With intuitive tools to design a robot's environment, robot creation becomes simpler. Virtual reality provides the best 3-dimensional visualization of real life, which makes for more intuitive design. Using virtual reality I created an easy-to-use tool that allows anyone to design a robotic environment. I developed a simple user interface that allows a user to design terrain 3-dimensionally. The design tool enables spawning, resizing, and placing multiple objects to form an environment that a robot may travel through. The tool extracts a numerical measurement of each object when resizing, allowing for scaled design necessary for practical robotic simulation. Overall, the tool simplifies environmental design and can help those who may not be well versed in robotics. With my simplified environmental design tool, future work involving structural design automation will allow nonexperts to create their own robots.

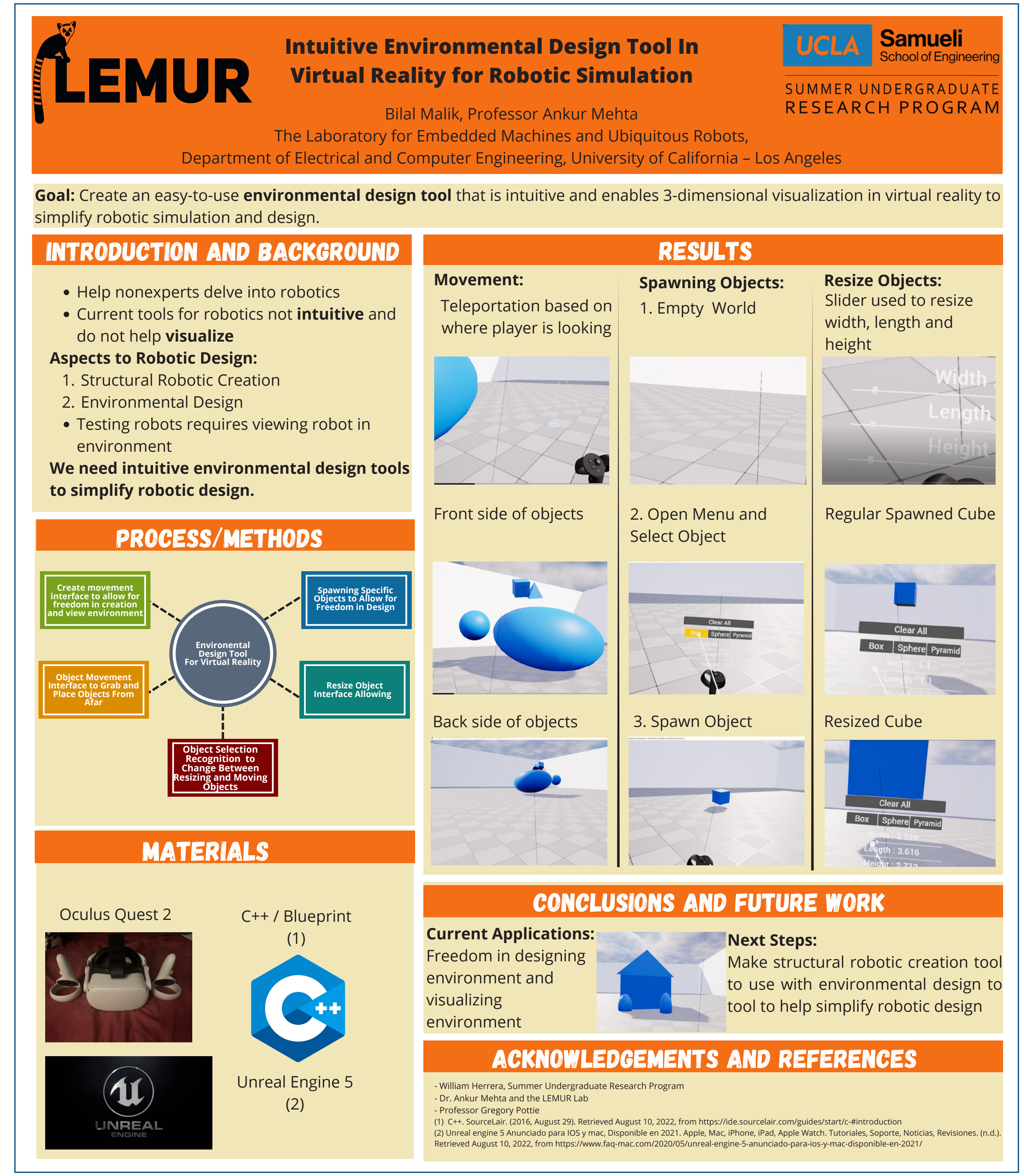

FACULTY ADVISOR
Yuzhang Li

DAILY LAB SUPERVISOR
Jiayi Yu

DEPARTMENT
Chemical and Biomolecular Engineering

MATTHEW MARGASON

Chemical and Biomolecular Engineering

3rd Year, UCLA

Measuring, Prediction, and Application of Pressure Profiles for Lithium-ion Batteries

ABSTRACT

In this project, we create a setup to measure the pressure profile of eight lithium-ion batteries simultaneously that can be charging at different protocols. We then collect cycling and pressure data and use this data to train a machine learning model that can be used for prediction of pressure profiles. We then seek to create a dynamic charging protocol using a PID control with our machine learning predictions in loop. We found that pressure has distinct behavior that can be used for many applications. Our preliminary results show that our machine learning model is accurate for the data we have but needs more data and more tuning to be accurate on a wider range. Our early PID control implementation shows that fast charging can be done with a smaller percentage of time causing lithium plating, but more tuning is needed to use this protocol for complete prevention of lithium plating. This work improves upon the slow constant current-constant voltage charging conventionally done. This will allow for increased charging rates, decreasing the required charging time. In addition, future experimentation will explore the use of machine learning predicted pressure profiles as a means of estimating battery lifetime. Differential pressure sensing, machine learning predictions, and PID control implementation will allow batteries to be charged faster and last longer.

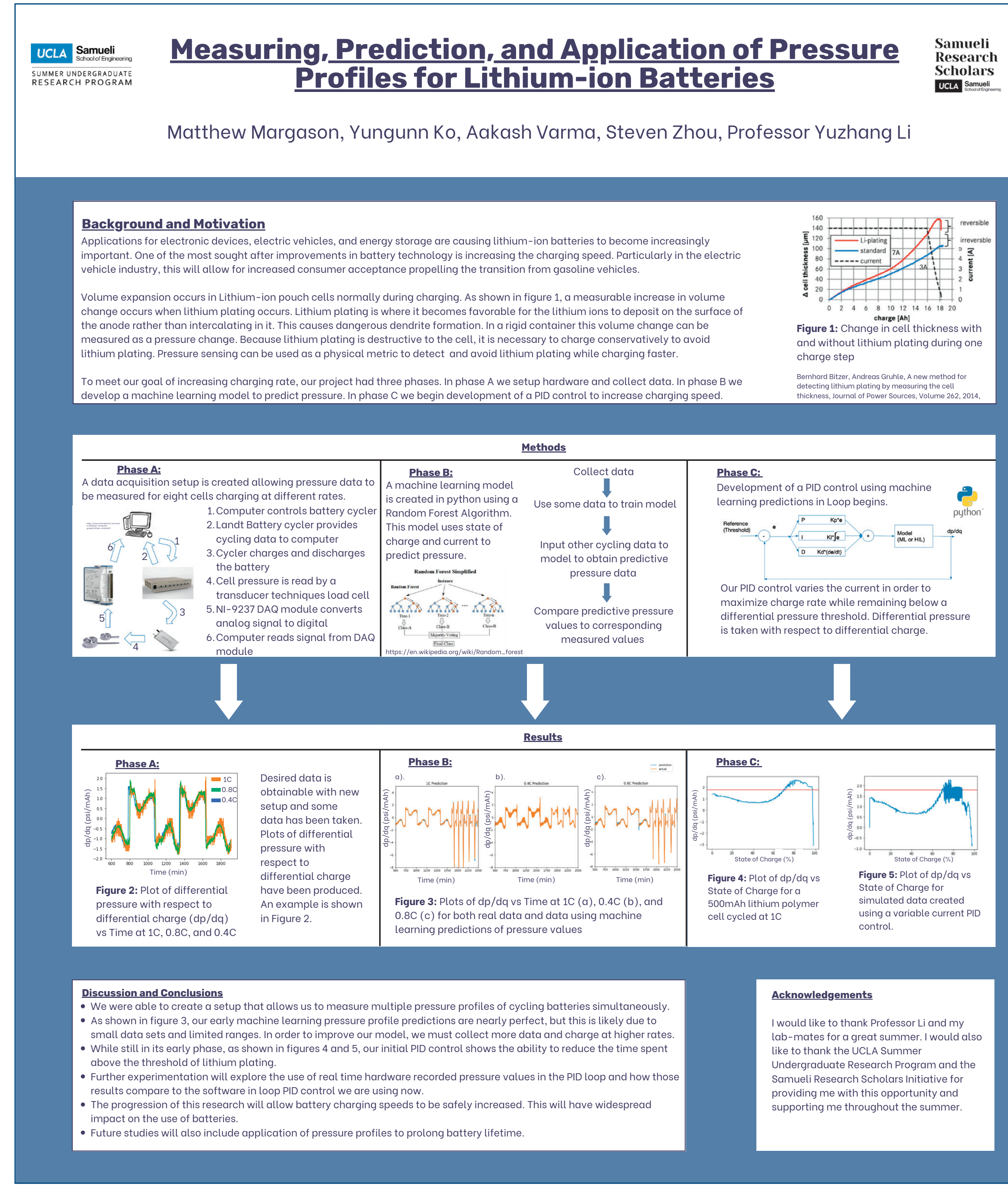

FACULTY ADVISOR
Tyler Clites

DAILY LAB SUPERVISOR
Brandon Peterson

DEPARTMENT
Mechanical and Aerospace Engineering

JOHN MCCULLOUGH

Mechanical and Aerospace Engineering

3rd Year, UCLA

Design and Modeling of Application-Specific Caged Hinges

ABSTRACT

Compliant mechanisms are parts or systems of parts that flex and bend to achieve desired motions. They are often manufactured as a single piece, eliminating sliding and rubbing motions between separate components; this significantly reduces wear and friction. As a result, compliant mechanisms require less maintenance and can be designed to have a longer lifespan than dynamically-equivalent, rigid mechanisms. Additionally, compliant mechanisms are incredibly precise, and can maintain this high precision throughout their entire lifespan. Consequently, in fields where maintenance, lifespan, and precision are top priorities, compliant mechanisms may be superior to rigid, over-constrained alternatives. A caged hinge is a particular type of compliant mechanism that permits rotation about one axis via elastic deformation, while remaining strong in tension along that same axis. Caged hinges have applications in industrial robot arms, wind turbines, satellites, and medical devices. However, there is currently no analytical tool to assist in the design of application-specific caged hinges. In this work, we present a model for predicting maximum stress in caged hinges of different sizes. More specifically, our model maps the relationship between geometry and load to both maximum stress and rotational stiffness. To build this model, we first performed finite element analysis (FEA) in ABAQUS on 65 mechanisms of different geometries, under varying loads. We then used linear-regression gradient-descent optimizations and simple neural networks to construct a multi-step model. Our model predicts maximum stress within a margin of error of 5% compared to FEA results. Future work includes validating stiffness values and using our model to determine the optimal caged hinge geometry for various prosthetics applications.

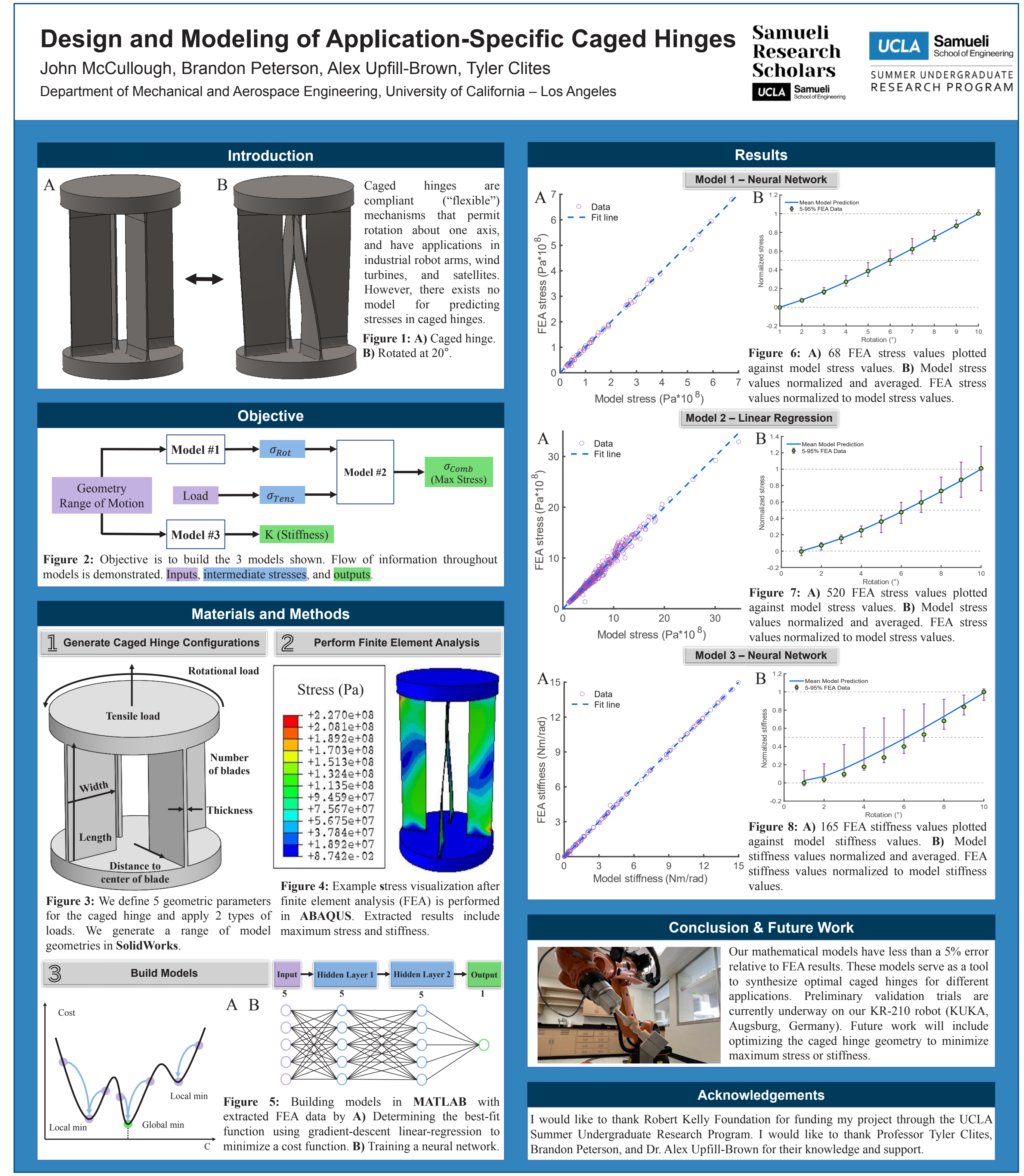

EUGENE MIN

Electrical and Computer Engineering

2nd Year, UCLA

ZIHAN QU

Electrical and Computer Engineering

3rd Year, UCLA

FACULTY ADVISOR

Richard Wesel

DAILY LAB SUPERVISOR

Linfang Wang

DEPARTMENT

Electrical and Computer Engineering

A Distribution Matcher for Asymmetric Probabilistic Amplitude Shaping

ABSTRACT

A communication system, which consists of a transmitter and a receiver, models the process by which the information is sent and received. The transmitted symbols that are generated by a transmitter go through a noisy channel and reach the receiver end. The receiver needs to estimate the transmitted symbols by their noisy version. Claude Shannon developed a theory that determines the maximum rate at which the receiver can reliably estimate the transmitted symbols based on the noise's statistics. To achieve the maximum rate, the transmitted signals need to approximately follow an optimal probability distribution, which can be done through probabilistic shaping. One method for probabilistic shaping is using a distribution matcher that takes a sequence of bits equally likely to be ones and zeros and maps it bijectively to a new sequence of symbols with the desired probability distribution.There are two types of distribution matchers denoted as constant and multi-composition distribution matchers or CCDMs and MCDMs. We coded a CCDM and a MCDM, which is a union of CCDMs. Two different versions of the MCDM based on a high probability and typical set rule were constructed. We found that MCDMs outperformed CCDMs in both normalized Kullback–Leibler (KL) divergence, a measure of how well the desired distribution is met, and matching rate, meaning we can send more information using less bits. By applying MCDMs to channels, we can achieve higher transmission rates and better noise correction to increase the efficiency and speed of the internet and communication systems around the world.

A Distribution Matcher for Asymmetric Probabilistic Amplitude Shaping

Zihan Qu, Eugene Min, Linfang Wang, Professor Richard Wesel
Department of Electrical and Computer Engineering, UCLA

SUMMER UNDERGRADUATE RESEARCH PROGRAM

FAST TRACK TO SUCCESS
UCLA Electrical and Computer Engineering

Introduction

Communication systems describe the way by which we transmit and receive information.

Binary communication systems use on and off bits represented by zeros and ones. Errors in a binary communication channel otherwise known as noise can flip a one to a zero.

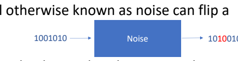

Claude Shannon developed a theory that determines the optimal probability distribution to reach maximum transmission rates.

Objective

Our objective is to make a distribution matcher that will make transmitted signals approximately follow an optimal probability distribution.

Principles

Communication System

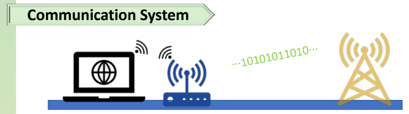

Figure 1: A system of a computer, a modem, and a cell tower is a simple communication system. Information is transmitted in a binary form.

Probabilistic Shaping

Probabilistic Shaping (PS) optimizes the shape and probability mass function (PMF) of a constellation set. This allows us to achieve optimal transmission rates.

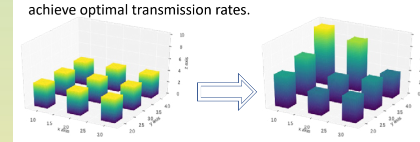

Figure 2: Probabilistic Shaping. 2(a) displays the PMF before Probabilistic Shaping and 2(b) displays the PMF after PS.

Distribution Matcher

A Distribution Matcher maps Bernoulli($\frac{1}{2}$) distributed input bits into a sequence of output symbols that follows a desired distribution. A Constant Composition Distribution Matcher (CCDM), can only map to one type of codeword distribution.

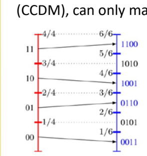

Figure 3: CCDM encoding mapping. 2-bit inputs are mapped bijectively to 4-bit codewords that follow a desired distribution. [2]

A Multi-Composition Distribution Matcher (MCDM), which is a union of CCDMs, permits more accurate distributions.

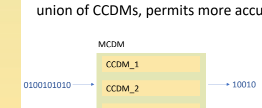

Figure 4: Outline of a MCDM structure with a 10-bit input and a 5-bit output codeword.

Materials

We implemented the CCDM and MCDMs in **C++**, a general-purpose programming language for development. We created helper functions to **determine MCDM thresholds and mitigate numerical overflow issues.**

Plots were generated using **Python**, a high-level, interpreted, general-purpose programming language, and **matplotlib.pyplot**, a library for creating static, animated, and interactive visualizations.

Mathematical Methods

SECTION I: Choosing Children Codebooks

Highest Probability Rule

$$P(A_i) = \underset{P(A^*)\in P\setminus\{P(A_1),\ldots,P(A_{i-1})\}}{\operatorname{argmax}} \sum_{a=1}^{|A|} P_{A^*}(a)\log P_{\hat{A}}(a)$$

The **Highest Probability (HP)** Rule ranks the CCDM codebooks based on most likely sequence of bits to occur. In **Table 1**, if P(1) = 0.8, then the most likely 4 bit output sequence is 1111 because the probability of 1111 occurring is 0.8*0.8*0.8*0.8.

Typical Set Rule

$$P(A_i) = \underset{P(A^*)\in P\setminus\{P(A_1),\ldots,P(A_{i-1})\}}{\operatorname{argmin}} D_{KL}(P(A^*)||P(\hat{A}))$$

The **Typical Set (TS)** Rule ranks the CCDM codebooks based on the output distribution's "distance" to the target distribution. In **Table 2**, if P(1) = 0.8 the closest distribution is one with 3 1's and 1 0's because for this distribution P(1) = 0.75.

# 0's	# 1's
0	4
1	3
2	2
3	1
4	0

Table 1: CCDMs ranked based on HP Rule

# 0's	# 1's
1	3
2	2
0	4
3	1
4	0

Table 2: CCDMs ranked based on TS Rule

SECTION II: Evaluation Metrics

KL Divergence

$$D(P_{\hat{A}}||P_A) = \sum_{a\in supp(P_A)} P_{\hat{A}}(a)\log_2\frac{P_{\hat{A}}(a)}{P_A(a)}$$

KL Divergence, also known as relative entropy, is one type of statistical distance between two distributions. Intuitively, it measures the difference between two distributions. Lower KL Divergence indicates the two distributions match better.

Normalized KL Divergence

$$\frac{D(P_{\hat{A}}||P_A)}{n} = -\frac{1}{n}\log_2|c| + H(P(\hat{A})) + D(P_{\hat{A}}||P_A)$$

The performance of a distribution matcher is measured by Normalized KL Divergence. Since the size of a codebook grows exponentially, the first term in the Normalized KL Divergence counteracts that effect.

Matching Rate

The **Matching Rate (MR)**, or transmission rate, is defined as $\frac{k}{n}$, with k being the length of input bits and n being the length of output symbols or codewords. We do not consider compressing the data, hence MR is less than 1. Higher MR in CCDM indicates more efficient encoding.

Results

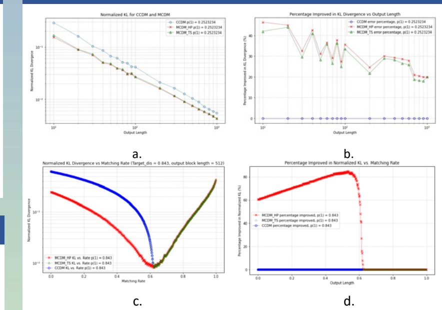

Figure 4: The performance of all three different types of distribution matchers are illustrated. 4(a) depicts the performance under specific output block lengths and 4(c) depicts the performance for specific matching rates. 4(b) and 4(d) quantifies the improvement in Normalized KL divergence.

- According to 4(b) the MCDMs had a 40% better performance in the 10-50 block length range, 30% in the 60-100 range and 20% in the 100-1,000 range than the CCDM.
- MCDM HP performed only around 2% better than MCDM TS.
- Based on 4(d), the MCDM TS and CCDM in the matching rate range of 0 to 0.62 performs 60%-80% worse than MCDM HP. For matching rates past the CCDM's capabilities, MCDM TS and HP perform similarly.

Conclusions

For matching rate, the MCDM TS utilizes the CCDM up to a matching rate of around .62, thus we see that their performance is equivalent in that range. However, the MCDM TS is favored because it can achieve higher matching rates. The MCDM HP clearly outperforms the CCDM.

After a matching rate of 0.62, MCDM HP or TS can be used. Before a matching rate of 0.62, the MCDM HP should be used.

Future Directions

By applying MCDMs to optical channels, we can achieve higher transmission rates and better noise correction. This increases the efficiency and speed of the internet and space systems.

References

[1] Linfang Wang, Dan Song, Felipe Areces, Thomas Wiegart, and Richard D. Wesel, "Probabilistic Shaping for Trellis-Coded Modulation with CRC-Aided List Decoding"
[2] P. Schulte and G. Böcherer, "Constant composition distribution matching," IEEE Trans. on Info. Theory, vol. 62, no. 1, pp. 430–434, 2015.
[3] Pikus, Marcin & Xu, Wen. (2019). "Arithmetic Coding Based Multi-Composition Codes for Bit-Level Distribution Matching." [Online]. Available: https://arxiv.org/pdf/1904.01819.pdf

Acknowledgements

This work was supported by the National Science Foundation through grant CCF 1911166 and by a Qualcomm Research Award. We would like to thank Professor Richard Wesel and Linfang Wang for providing guidance and mentorship during the research. We would also like to Will Herrera for organizing the SURP program.

FACULTY ADVISOR
Danijela Cabric

DAILY LAB SUPERVISOR
Shamik Sarkar

DEPARTMENT
Electrical and Computer Engineering

VIDHYA PRABHU

Electrical and Computer Engineering

1st Year, UCLA

Proactive Signal Strength using 2D Deep Learning Model

ABSTRACT

An essential tool to furthering dynamic spectrum sharing, which allocates spectrum based on user demand, is knowing the signal strength on particular frequencies and at locations, allowing optimized base station placement for efficient use of the spectrum between many devices in an area. Given the location of existing fixed transmitters and the locations and signal strength of their respective receivers, our goal is to find the signal strength at any point in an area of interest due to a transmitter at any location, but without any active transmission from the transmitter. The path loss model, employing a least squares linear regression, is a traditional method for this problem; however, finding the signal strength in an urban area, because of building obstacles, has a complex pattern of loss, so we attempt to predict that strength through a deep learning model. Specifically, we use a 2D format to feed in data, ideally giving the model spatial context of multiple receivers' signal strengths at once. We use the U-Net architecture, which is a type of convolutional neural network with an image-to-image translation: the input is two matrices, one representing the transmitter location and the other representing all the receivers' locations, and the output is an image of the predicted signal strengths at the receiver locations used in the input. Using simulation-based evaluation, we find that, on using a wide range of available transmitters and receivers to train the model, this method does achieve a more accurate prediction of signal strength than the path loss model. Future work includes tuning this model with additional information, such as the area's terrain and buildings, and verifying results with real data collected or crowdsourced, instead of using datasets obtained through simulations.

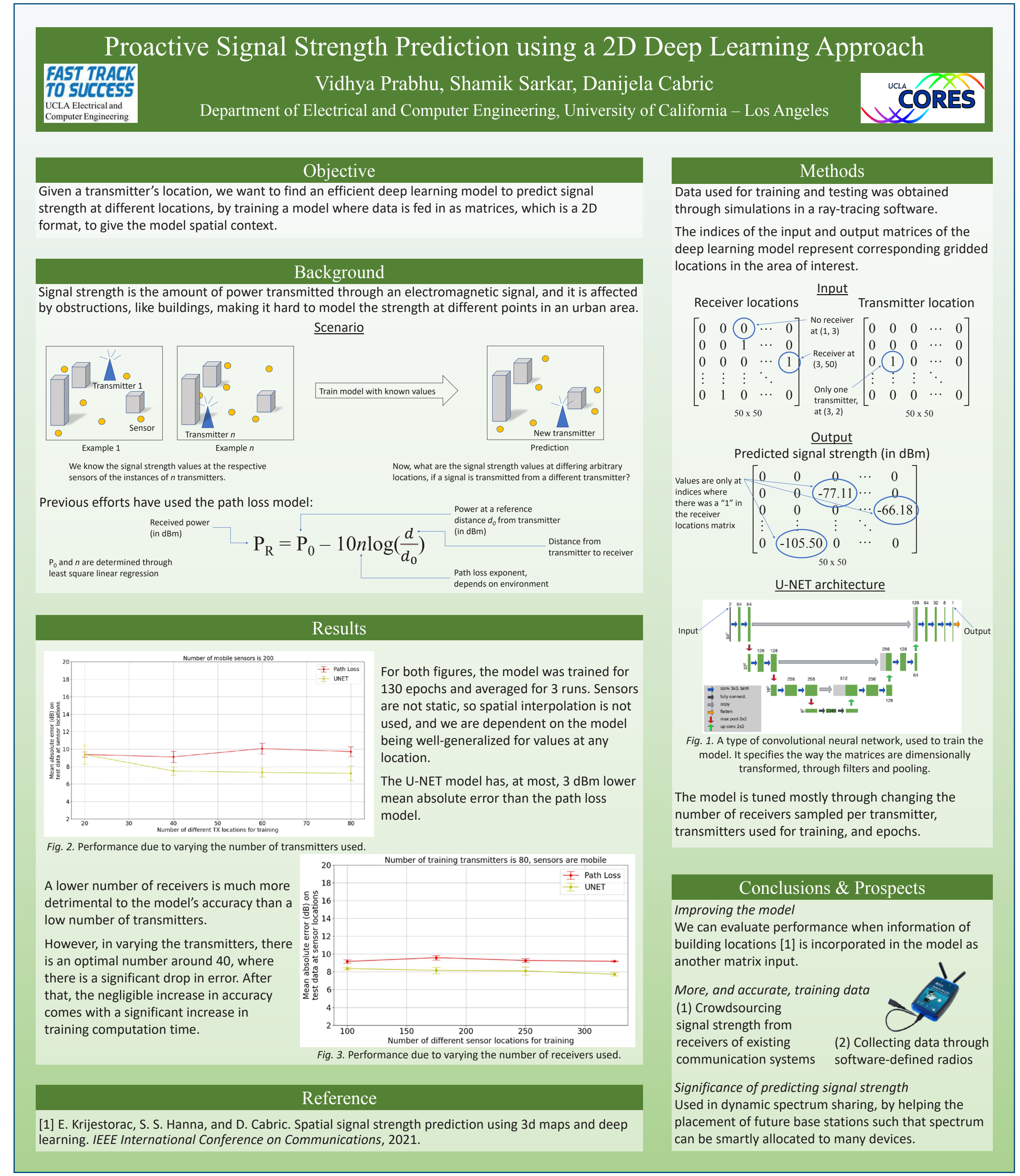

ARTURO RAMIREZ

Physics

4th Year, CSUN

FACULTY ADVISOR
Chee Wei Wong

DAILY LAB SUPERVISORS
Jin Ho Kang, Jiahui Huang

DEPARTMENT
Electrical and Computer Engineering

Phonon Modes and Raman Signatures of MnBiTe Magnetc Topological Heterostructure

ABSTRACT

The intersection of magnetism and topological electronic structure in momentum space has gained great interest in the field of condensed matter physics and quantum electronics. There has been great effort in observing magnetic ordering within 2D and quasi-2D materials since their discovery. Novel phenomena such as the anomalous quantum Hall effect, Weyl Fermions and axion insulator phases can be realized in such systems, only that it has proven difficult to engineer well controlled doping concentrations over large areas. MnBi2Te4 and its family MnBi2nTe3n+1 overcome these difficulties as it is easily synthesized into uniform bulk single crystals. Using a laser, photons are directed onto the MnBi2Te4 sample to have its back scattered photons collected and sorted by wavelength within a spectrometer. A charge couple device then detects the number of photons, or intensity, per wavelength to provide a unique signature of the molecule. The Raman signatures of MnBi2Te4 demonstrate the E modes at 27 cm-1, 67 cm-1, & 104 cm-1 and A modes at 47 cm-1, 124 cm-1 and 140 cm-1 with the newly observed E mode peak measured at 27cm-1. A 1D scan of the MnBi2Te4 is performed on silicon substrate using a motorized stage to provide a gradient of each material's intensity across the sample's surface. With this enhancement of the Raman spectrum to MBT-124, the pronouncement of the vibrational modes will provide a new scope in observing its magnetic ordering when subjected to a range of cryogenic temperature and magnetic field variances.

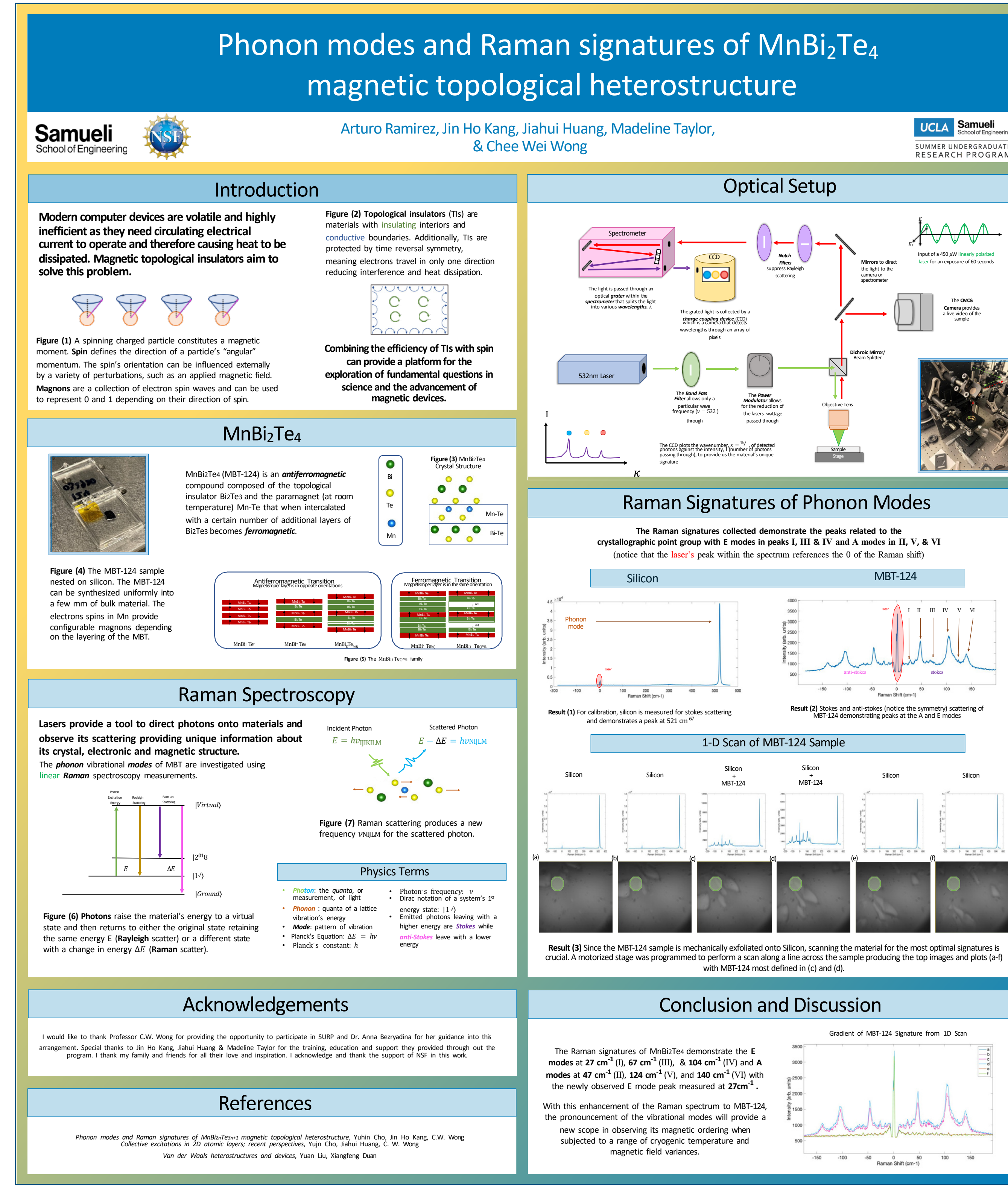

FACULTY ADVISOR
Neil Lin

DAILY LAB SUPERVISOR
Marie Payne

DEPARTMENT
Mechanical and Aerospace Engineering

MELISSA RUPERT

Bioengineering

3rd Year, UCLA

Revealing Effects of Physiological Stimuli on Neuroepithelial Development in Forebrain Organoids

ABSTRACT

Human brain organoid models create unprecedented opportunities for study of neurological diseases and early neurologic development. Unfortunately, such a promising system often exhibits impaired growth and suboptimal structure in traditional culture due to the insufficient diffusion of oxygen and nutrients within organoids. To improve solute transport and supply, many engineering tools including hyperoxic incubation and fluidic flow have been routinely incorporated in organoid culture. While these physiological stimuli are known to play an equally important role as their chemical counterparts (e.g., growth factors), their impacts on organoid development are relatively undefined. As a result, effectively engineering the culture microenvironment to optimize organoid differentiation remains challenging. We investigated the individual and combined impacts of flow and hyperoxia, two essential solute transport enhancement tools, by culturing forebrain organoids either in static wells or in our unique culture device in both normoxic and hyperoxic environments. The samples were collected at various time points for various characterizations. Compared to the static normoxia control, we found that organoids cultured in flow and hyperoxia had a significant increase in size and neural architecture, with the maximal benefit imparted by both stimuli together (i.e., flow + hyperoxia). We observed that flow led to an enhanced growth of the cortical plate region due to increased mechanotransduction on the periphery of the organoids. Our results suggest that flow and hyperoxia culture produce structurally improved organoids, suggesting the importance of modulating environmental stimulation in organoid differentiation.

Revealing Effects of Physiological Stimuli on Neuroepithelial Development in Forebrain Organoids

Melissa Rupert[1], Marie Payne[2], Nathan Cai[1], Kathryn Saxton[1], Neil Lin[12]

[1]Dept. of Bioengineering, [2]Dept. of Mechanical & Aerospace Engineering, University of California, Los Angeles

UCLA Samueli School of Engineering

SUMMER UNDERGRADUATE RESEARCH PROGRAM

Samueli Research Scholars

UCLA Samueli School of Engineering

Background

Human brain organoid models create unprecedented opportunities for study of neurological diseases and early neurologic development. Unfortunately, such a promising system often exhibits impaired growth and suboptimal structure in traditional culture due to the insufficient diffusion of oxygen and nutrients within organoids.

To improve solute transport and supply, many engineering tools including hyperoxic incubation and fluidic flow have been routinely incorporated in organoid culture[12]. While these physiological stimuli are known to play an equally important role as their chemical counterparts (e.g., growth factors), their impacts on organoid development are relatively undefined. As a result, effectively engineering the culture microenvironment to optimize organoid differentiation remains challenging.

Materials & Methods

We investigated the individual and combined impacts of flow and hyperoxia, two essential solute transport enhancement tools, by culturing forebrain organoids either in static wells or in our Microwell Flow Device (MFD) in both normoxic and hyperoxic environments.

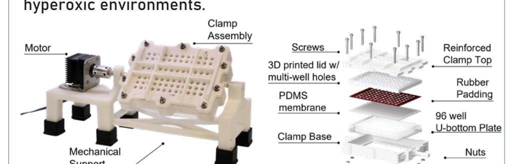

Figure 1. Microwell Flow Device. Our culture device for applying gravity-induced shear stress to the organoids, and an expanded view of the clamping system used to create a water-tight seal in the 96 well plate.

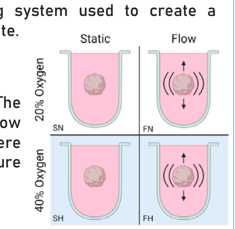

Figure 2. Culture conditions. The environmental factors of static/flow and normoxia/hyperoxia were paired to create four distinct culture conditions to compare.

Forebrain organoids were obtained at day 18 and separated into the four conditions until day 56. The samples were collected at various time points for RNA analysis, metabolomics, or immunoimaging.

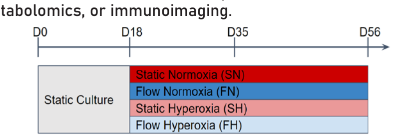

Figure 3. Experimental timeline. Organoids were cultured statically from seeding until day 18, when they were transferred to one of our 4 experimental conditions. Important physiological timepoints include D35 and D56.

Results

Flow and hyperoxia have additive effects on enhancing organoid growth.

Brightfield images were taken of organoids in each condition, and the cross-sectional area fold change from the initial size was measured to quantify growth. Organoids subjected to either flow or hyperoxia independently increased growth, and organoids subjected to a combination of fluidic flow and hyperoxia displayed the most significant growth.

In addition, when immunostaining was done for neural progenitor marker FOXG1 and adhesion junction marker NCAD, longer neural rosettes were seen in higher numbers in the flow hyperoxia condition.

These results suggest that the mechanisms by which flow and hyperoxia operate to enhance organoid growth are separate, allowing for additive benefits when performed in combination.

Cortical plate growth is enhanced by flow.

The ventricular (VZ), subventricular (SVZ), and cortical plate (CP) regions of the organoids were visualized by staining for PAX6, TBR2, and CTIP2, respectively. The VZ and SVZ layer thickness were consistent across conditions, but the CP had a higher thickness in flow conditions.

This could suggest that one of the mechanisms by which flow operates is through increased mechanotransduction on the periphery of the organoids, enhancing growth.

Unique metabolic profiles are generated in each condition.

When a metabolism assay was run, organoids in all condition consumed similar metabolites, but the level at which they consumed each metabolite was different. Flow and hyperoxia independently shifted the metabolic phenotype to show an increased consumption of several more metabolites than static normoxia, while the flow hyperoxia condition had many more significantly consumed metabolites, displaying a more diversified consumption profile.

Conclusions & Future Directions

Compared to the static normoxia control, we found that organoids cultured in flow normoxia and static hyperoxia, respectively, had a significant increase in size and neural rosette structure, with the maximal benefit imparted by both stimuli together (i.e., flow + hyperoxia). We observed that flow increased the thickness of the cortical plate on the periphery of the organoids, suggesting that flow increases mechanotransduction on cells in the periphery, causing the enhanced layer growth.

We also saw that flow and hyperoxia induced a metabolic change on the organoids, changing the diversity of consumed metabolites. The shifted profiles demonstrate how flow and hyperoxia may cause an upregulation of other metabolic pathways, increasing organoid growth.

Our results suggest that flow and hyperoxia culture produce structurally improved organoids, suggesting the importance of modulating environmental stimulation in organoid differentiation. Future directions for our work include performing RNAseq to verify upstream responses to physiological stimuli match our observed downstream responses, as well as staining for oxidative/glycolytic stress markers to analyze the effects of flow/hyperoxia on organoid growth.

References

1. Watanabe, M. *et al.* Self-Organized Cerebral Organoids with Human-Specific Features Predict Effective Drugs to Combat Zika Virus Infection. *Cell Reports* 21, 517–532 (2017).
2. Qian, X. *et al.* Brain-Region-Specific Organoids Using Mini-bioreactors for Modeling ZIKV Exposure. *Cell* 165, 1238–1254 (2016).

Acknowledgements

I want to thank my PI Neil Lin along with my graduate student mentor Marie Payne for supporting me throughout this project. I also want to thank my fellow lab members Nathan Cai and Kathryn Saxton for all the work they have contributed to this project. I also want to thank the Novitch lab for providing us with organoid samples and reagents and for providing us feedback.

SUDARSHAN SESHADRI

Electrical and Computer Engineering

2nd Year, UCLA

ARTHUR YANG

Electrical and Computer Engineering

1st Year, UCLA

FACULTY ADVISOR

Richard Wesel

DAILY LAB SUPERVISOR

Richard Wesel

DEPARTMENT

Electrical and Computer Engineering

Implementation of AR4JA LDPC Encoding and Decoding Using min* Algorithm

ABSTRACT

Low Density Parity Check (LDPC) codes are linear block codes with high throughput and error-correction capabilities, making them relevant for transmission of information over constrained or noisy transmission channels in communications. Iterative message passing algorithms are used to decode LDPC codes passed between variable nodes corresponding to the received channel bits and check nodes. While Sum-Product Algorithm (SPA) achieves high decoding performance at the expense of high computational complexity, reduced complexity decoding algorithms such as Min-Sum Algorithm (MSA) meanwhile can suffer decoding performance degradation as a tradeoff for simplified computation of outgoing check node messages. Through an implementation of a modified MSA with correction term, also known as min* algorithm, in a LDPC decoding on both software and hardware, we seek to demonstrate and verify improved decoding performance over MSA. The min* LDPC decoder is implemented in a MATLAB testing script via a forward-backward algorithm -based message passing operation, demonstrating clear improved performance over standard min-sum decoding in both bit-error-rate (BER) tests for parameters of 100 trials, 50 maximum iterations and frame-error rate (FER) tests measures across set parameters of 20 error frames calculation threshold, 20 maximum iterations. BER and FER curves generated from these tests verify the postulation of improved decoding performance in min*- based LDPC decoding over min-sum LDPC decoding. Future work is expected to continue on the development of a hardware-based min* LDPC decoder that is being written in SystemVerilog to run on a ZCU106 FPGA.

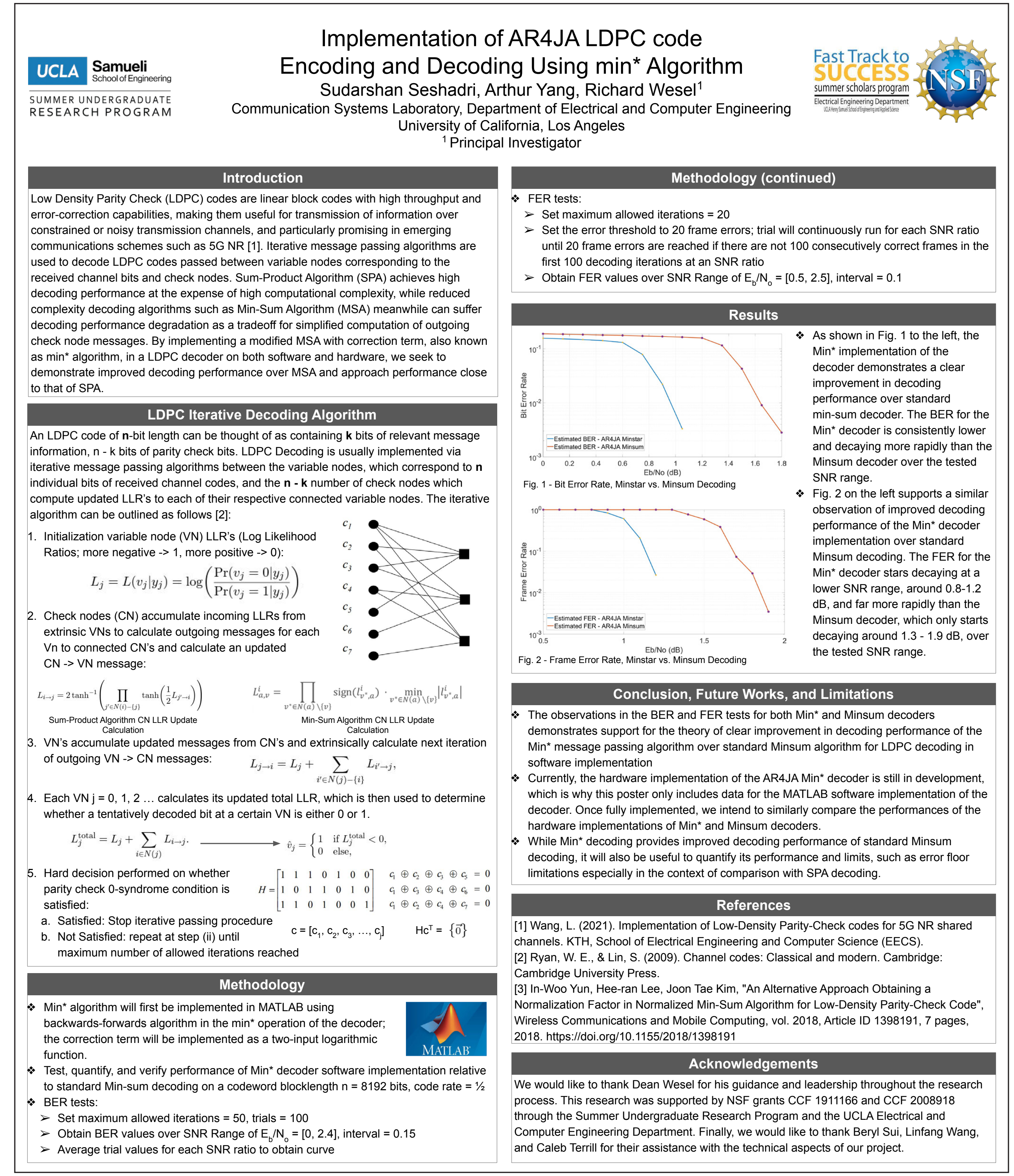

Implementation of AR4JA LDPC code Encoding and Decoding Using min* Algorithm

Sudarshan Seshadri, Arthur Yang, Richard Wesel[1]

Communication Systems Laboratory, Department of Electrical and Computer Engineering

University of California, Los Angeles

[1] Principal Investigator

Introduction

Low Density Parity Check (LDPC) codes are linear block codes with high throughput and error-correction capabilities, making them useful for transmission of information over constrained or noisy transmission channels, and particularly promising in emerging communications schemes such as 5G NR [1]. Iterative message passing algorithms are used to decode LDPC codes passed between variable nodes corresponding to the received channel bits and check nodes. Sum-Product Algorithm (SPA) achieves high decoding performance at the expense of high computational complexity, while reduced complexity decoding algorithms such as Min-Sum Algorithm (MSA) meanwhile can suffer decoding performance degradation as a tradeoff for simplified computation of outgoing check node messages. By implementing a modified MSA with correction term, also known as min* algorithm, in a LDPC decoder on both software and hardware, we seek to demonstrate improved decoding performance over MSA and approach performance close to that of SPA.

LDPC Iterative Decoding Algorithm

An LDPC code of **n**-bit length can be thought of as containing **k** bits of relevant message information, n - k bits of parity check bits. LDPC Decoding is usually implemented via iterative message passing algorithms between the variable nodes, which correspond to **n** individual bits of received channel codes, and the **n - k** number of check nodes which compute updated LLR's to each of their respective connected variable nodes. The iterative algorithm can be outlined as follows [2]:

1. Initialization variable node (VN) LLR's (Log Likelihood Ratios; more negative -> 1, more positive -> 0):

$$L_j = L(v_j|y_j) = \log\left(\frac{\Pr(v_j = 0|y_j)}{\Pr(v_j = 1|y_j)}\right)$$

c_1 c_2 c_3 c_4 c_5 c_6 c_7

2. Check nodes (CN) accumulate incoming LLRs from extrinsic VNs to calculate outgoing messages for each Vn to connected CN's and calculate an updated CN -> VN message:

$$L_{i\to j} = 2\tanh^{-1}\left(\prod_{j'\in N(i)-\{j\}} \tanh\left(\frac{1}{2}L_{j'\to i}\right)\right)$$

Sum-Product Algorithm CN LLR Update Calculation

$$L^i_{a,v} = \prod_{v^*\in N(a)\backslash\{v\}} \mathrm{sign}(l^i_{v^*,a}) \cdot \min_{v^*\in N(a)\backslash\{v\}} |l^i_{v^*,a}|$$

Min-Sum Algorithm CN LLR Update Calculation

3. VN's accumulate updated messages from CN's and extrinsically calculate next iteration of outgoing VN -> CN messages:

$$L_{j\to i} = L_j + \sum_{i'\in N(j)-\{i\}} L_{i'\to j},$$

4. Each VN j = 0, 1, 2 … calculates its updated total LLR, which is then used to determine whether a tentatively decoded bit at a certain VN is either 0 or 1.

$$L_j^{\text{total}} = L_j + \sum_{i\in N(j)} L_{i\to j}. \longrightarrow \hat{v}_j = \begin{cases} 1 & \text{if } L_j^{\text{total}} < 0, \\ 0 & \text{else,} \end{cases}$$

5. Hard decision performed on whether parity check 0-syndrome condition is satisfied:
   a. Satisfied: Stop iterative passing procedure
   b. Not Satisfied: repeat at step (ii) until maximum number of allowed iterations reached

$$H = \begin{bmatrix} 1 & 1 & 1 & 0 & 1 & 0 & 0 \\ 1 & 0 & 1 & 1 & 0 & 1 & 0 \\ 1 & 1 & 0 & 1 & 0 & 0 & 1 \end{bmatrix} \quad \begin{aligned} c_1 \oplus c_2 \oplus c_3 \oplus c_5 &= 0 \\ c_1 \oplus c_3 \oplus c_4 \oplus c_6 &= 0 \\ c_1 \oplus c_2 \oplus c_4 \oplus c_7 &= 0 \end{aligned}$$

$c = [c_1, c_2, c_3, \ldots, c_j]$ $\quad Hc^T = \{\vec{0}\}$

Methodology

- Min* algorithm will first be implemented in MATLAB using backwards-forwards algorithm in the min* operation of the decoder; the correction term will be implemented as a two-input logarithmic function.
- Test, quantify, and verify performance of Min* decoder software implementation relative to standard Min-sum decoding on a codeword blocklength n = 8192 bits, code rate = ½
- BER tests:
  - Set maximum allowed iterations = 50, trials = 100
  - Obtain BER values over SNR Range of E_b/N_o = [0, 2.4], interval = 0.15
  - Average trial values for each SNR ratio to obtain curve

Methodology (continued)

- FER tests:
  - Set maximum allowed iterations = 20
  - Set the error threshold to 20 frame errors; trial will continuously run for each SNR ratio until 20 frame errors are reached if there are not 100 consecutively correct frames in the first 100 decoding iterations at an SNR ratio
  - Obtain FER values over SNR Range of E_b/N_o = [0.5, 2.5], interval = 0.1

Results

Estimated BER - AR4JA Minstar
Estimated BER - AR4JA Minsum
Bit Error Rate
Eb/No (dB)

Fig. 1 - Bit Error Rate, Minstar vs. Minsum Decoding

Estimated FER - AR4JA Minstar
Estimated FER - AR4JA Minsum
Frame Error Rate
Eb/No (dB)

Fig. 2 - Frame Error Rate, Minstar vs. Minsum Decoding

- As shown in Fig. 1 to the left, the Min* implementation of the decoder demonstrates a clear improvement in decoding performance over standard min-sum decoder. The BER for the Min* decoder is consistently lower and decaying more rapidly than the Minsum decoder over the tested SNR range.
- Fig. 2 on the left supports a similar observation of improved decoding performance of the Min* decoder implementation over standard Minsum decoding. The FER for the Min* decoder stars decaying at a lower SNR range, around 0.8-1.2 dB, and far more rapidly than the Minsum decoder, which only starts decaying around 1.3 - 1.9 dB, over the tested SNR range.

Conclusion, Future Works, and Limitations

- The observations in the BER and FER tests for both Min* and Minsum decoders demonstrates support for the theory of clear improvement in decoding performance of the Min* message passing algorithm over standard Minsum algorithm for LDPC decoding in software implementation
- Currently, the hardware implementation of the AR4JA Min* decoder is still in development, which is why this poster only includes data for the MATLAB software implementation of the decoder. Once fully implemented, we intend to similarly compare the performances of the hardware implementations of Min* and Minsum decoders.
- While Min* decoding provides improved decoding performance of standard Minsum decoding, it will also be useful to quantify its performance and limits, such as error floor limitations especially in the context of comparison with SPA decoding.

References

[1] Wang, L. (2021). Implementation of Low-Density Parity-Check codes for 5G NR shared channels. KTH, School of Electrical Engineering and Computer Science (EECS).
[2] Ryan, W. E., & Lin, S. (2009). Channel codes: Classical and modern. Cambridge: Cambridge University Press.
[3] In-Woo Yun, Hee-ran Lee, Joon Tae Kim, "An Alternative Approach Obtaining a Normalization Factor in Normalized Min-Sum Algorithm for Low-Density Parity-Check Code", Wireless Communications and Mobile Computing, vol. 2018, Article ID 1398191, 7 pages, 2018. https://doi.org/10.1155/2018/1398191

Acknowledgements

We would like to thank Dean Wesel for his guidance and leadership throughout the research process. This research was supported by NSF grants CCF 1911166 and CCF 2008918 through the Summer Undergraduate Research Program and the UCLA Electrical and Computer Engineering Department. Finally, we would like to thank Beryl Sui, Linfang Wang, and Caleb Terrill for their assistance with the technical aspects of our project.

WILLIAM SHIH

Electrical and Computer Engineering

1st Year, UCLA

FACULTY ADVISOR

Ankur Mehta

DAILY LAB SUPERVISOR

Ankur Mehta

DEPARTMENT

Electrical and Computer Engineering

End-to-End Design Process for Cut-and-Fold Modular Robots

ABSTRACT

Robot development is a challenging and resource-consuming process requiring the integration of mechanical, electronic, and computational subsystems. In addition, many iterations of designing and testing are required to customize robotic technology to fit individual needs. Our goal is to increase accessibility and streamline the robot development process by using a modular approach to assembly. This would aid introductory-level roboticists in producing simple designs while facilitating their creativity. We use Robot Compiler (RoCo), a framework for visualizing and generating cut-and-fold robots whose mechanical parts are fabricated as flat sheets of material that can be easily folded into a prescribed 3D form. We compiled a library of modular robotic components that are relevant to ground locomotion. This database of parts enables designers to realize new robot designs which can be paired with electronics and software to simulate different types of ground locomotion such as rolling, crawling, and walking. We present some of the many potential robot designs that can be constructed to demonstrate this modular procedure of designing cut-and-fold robots with RoCo. Our research provides a rapid process that allows users to create affordable and versatile robots with a short turnaround time.

ANJALI SIVANANDAN

Bioengineering

3rd Year, UCLA

FACULTY ADVISOR
Jennifer Wilson

DAILY LAB SUPERVISOR
Jennifer Wilson

DEPARTMENT
Bioengineering

Utilizing PathFX to Analyze Drug-Gene Associations in Diabetes and Lung Cancer

ABSTRACT

Protein-Protein Interaction (PPI) network methods are an increasingly popular way to predict drug downstream effects. For example, PathFX is a novel alg rithm that uses PPI network methods to identify drug pathway associations and drug-related phenotypes. However, these algorithms often predict more drug effects than evidence supports. These predictions can be tested by conducting observational studies in the Electronic Health Record (EHR). However, instead of testing each individual drug-disease prediction in the EHR, it is more practical to test groups of drugs based on shared gene pathways. This study will focus on the specific disease areas of diabetes and lung cancer to illustrate how PathFX can be used to analyze drug-gene and drug-disease associations to identify hypotheses for shared drug-gene pathways. We analyzed PathFX networks for drugs used to treat diabetes and lung cancer. We analyzed the frequency of shared genes and shared phenotypes, and used downstream proteins to cluster treatment drugs. We identified 44 and 34 drugs for diabetes and lung cancer respectively, and found drug network clusters are distinct from ATC groups. We used GO enrichment to discover functions associated with network clusters and found that diabetes and lung cancer pathways had distinct functional categories. We hypothesize that we will be able to distinguish clinical and non-clinical drugs by their downstream pathways and provide a means to reduce PathFX over-prediction. We will later use observational studies in the EHR to test the utility of network-identified clusters and expand this analysis to other disease areas.

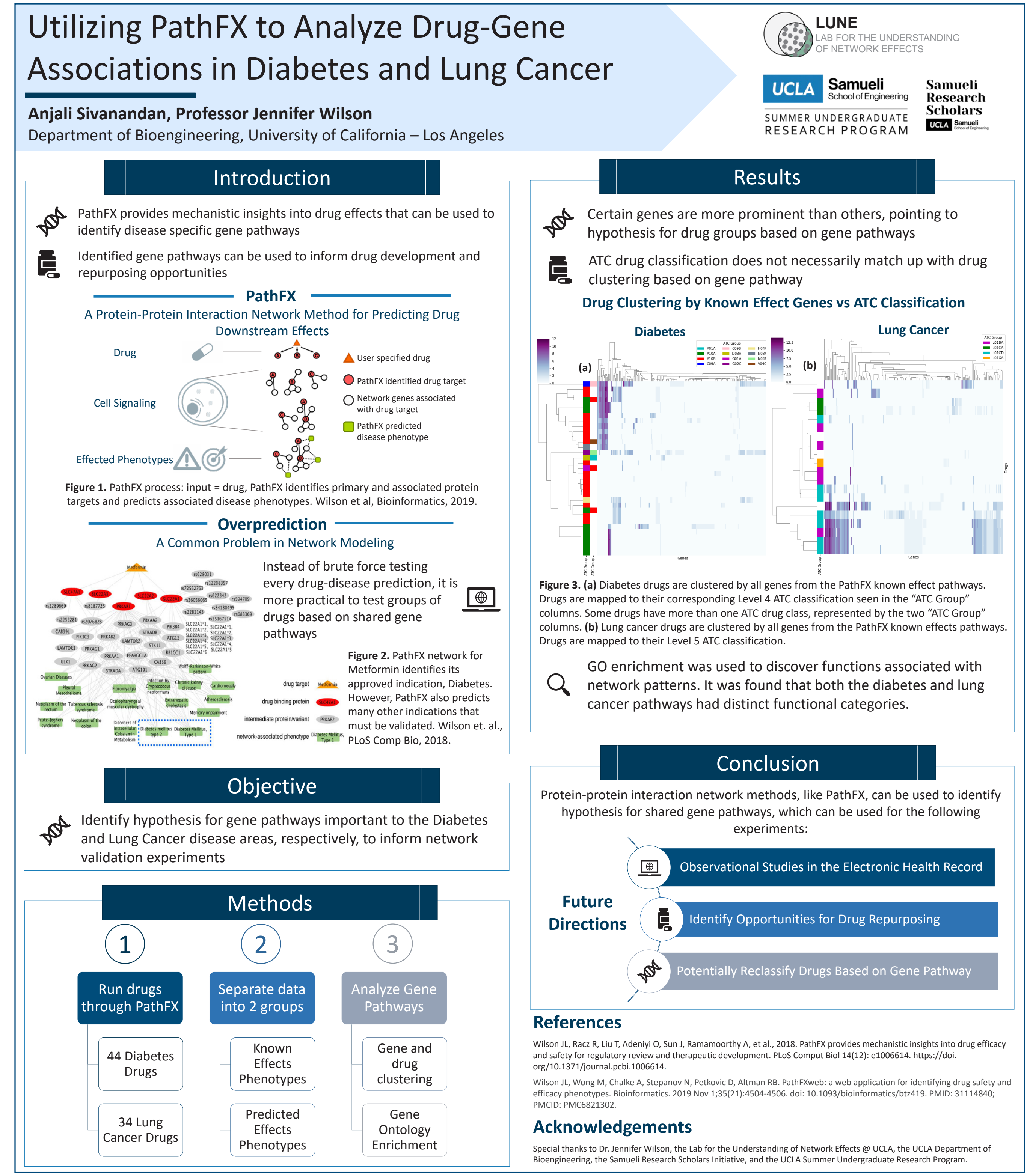

FACULTY ADVISOR
Rob Candler

DAILY LAB SUPERVISOR
Ben Pound

DEPARTMENT
Electrical and Computer Engineering

KATHERINE SOHN

Electrical and Computer Engineering

1st Year, UCLA

Current Sheet Quadrupole Focusing for Short-Period Undulators

ABSTRACT

X-ray free-electron lasers (XFELs) produce short, high-energy pulses of X-ray radiation by wiggling a beam of relativistic electrons through a magnetic array called an undulator. While these distinctly powerful X-ray pulses enable unprecedented research in a broad range of fields, XFELs are large, cost billions of dollars, and are only able to serve a few experiments at time, resulting in severely limited facility access. So-called "short-period" undulators have the potential to reduce the cost and size of an XFEL; however, these tend to be drastically less efficient than undulators with longer periods. One way to target this inefficiency is by focusing the electron beam as it passes through the undulator. This increases the efficiency of the FEL process, leading to a shorter overall undulator length and higher photon beam power, but previous techniques employing permanent magnets are not tunable and difficult to manufacture and align. We propose using copper current sheets instead, which are both tunable and simple to install. In this experiment, we investigate the practicality of this design through simulation and modeling. Our results illustrate the optimum width of current sheet at 4.75 mm for our chosen gap height of 2.5 mm, creating a "good field" region 2.4 mm wide while maintaining a gradient of 0.25 T/m at a small current density of 1.92e7 A/m^2. The gradient could reasonably be increased by two or three orders of magnitude with larger currents, commensurate with desired gradient levels in upcoming FELs.

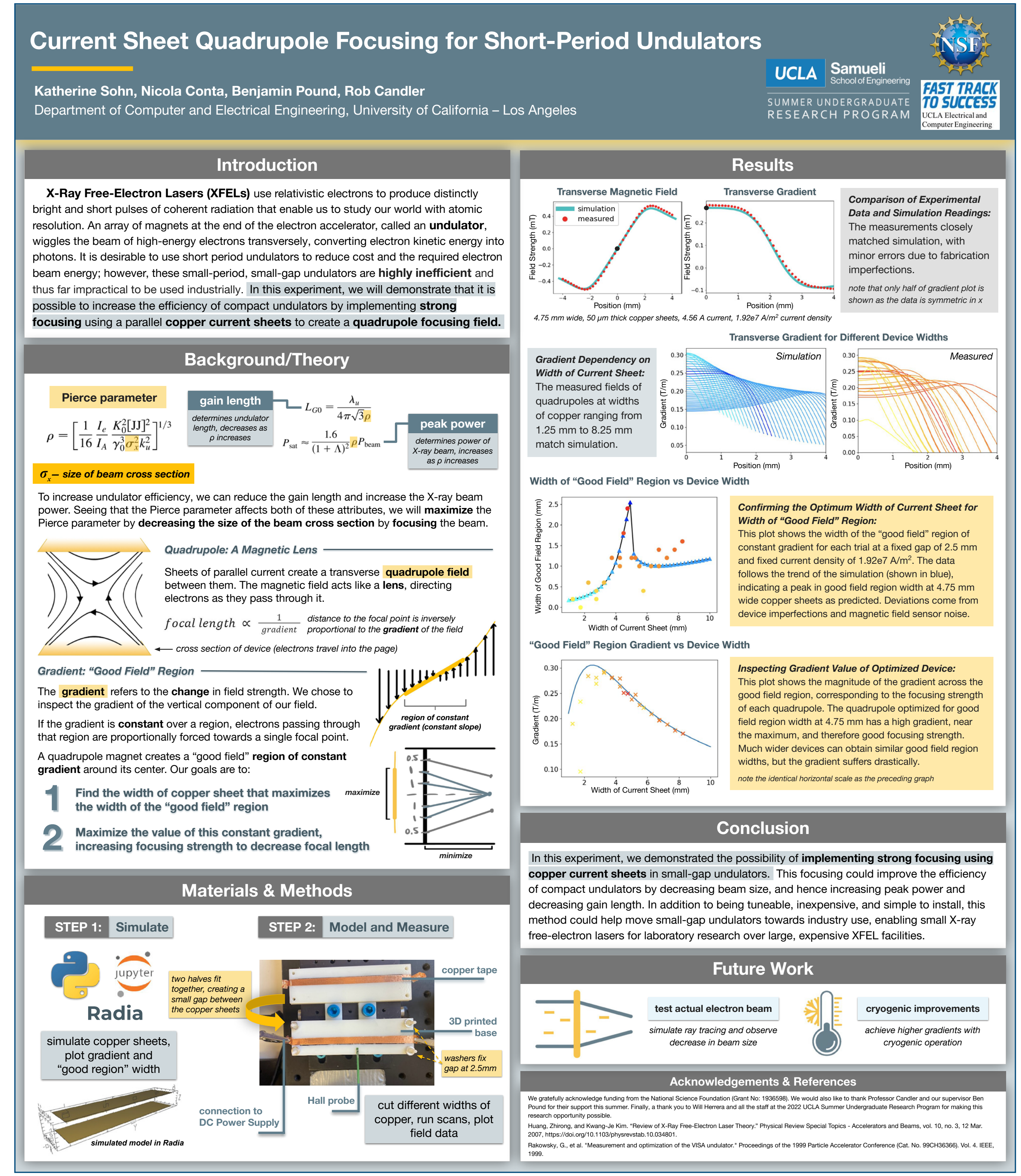

FACULTY ADVISOR
Yang Zhang

DAILY LAB SUPERVISOR
Siyou Pei

DEPARTMENT
Electrical and Computer Engineering

ANDERSON TRUONG

Electrical and Computer Engineering

2nd Year, UCLA

GroundSight: Floor-Sensing Shoe Wearable for Inferring User Location

ABSTRACT

Real-time location systems (RTLS) are increasingly being used in healthcare and warehouse facilities to monitor the activity of people and equipment. Unlike global positioning, RTLS are a type of local positioning system used for localization within a closed area. Most RTLS use large networks of transmitters and receivers, which can be very expensive to implement. The large overhead and cost make these systems inaccessible to users and smaller facilities with low budgets. Current RTLS solutions also raise privacy concerns with their constant surveillance and monitoring of user location data. To develop a more affordable and secure user localization method, position tracking and identification should be fully performed by the user without any external signals and allow them to control access to their location data. Here, we present a new localization method: GroundSight: a smart shoe accessory that coarsely tracks a user's positioning by sensing micro environments the user is in with discernable floor patterns. Attached to the heel, the low-profile wearable captures images of the ground in-sync with the user's steps. The device then classifies and matches these images to a set of user-defined locations in real-time and logs the location data in an SD card or the user's smartphone. The user is given full control over their location logs and has the choice to share their data. With affordable components and processing done all on-device, GroundSight offers a low-cost alternative to more expensive RTLS systems and an assurance on privacy and protection through user autonomy.

MIKAELA VAN DE HEETKAMP

Mechanical and Aerospace Engineering

1st Year, UCLA

FACULTY ADVISOR

Lihua Jin

DAILY LAB SUPERVISOR

Shivam Agarwal

DEPARTMENT

Mechanical and Aerospace Engineering

3D Printed Liquid Crystal Elastomers

ABSTRACT

Liquid crystal elastomers (LCEs) are soft stimuli-responsive materials that contract along the orientation of mesogen, called director, upon heating due to a transition from the nematic to isotropic phase. LCE structures can be utilized for applications requiring remote actuation, cyclic actuation and miniaturization. Direct Ink Writing 3D printing allows fabrication of LCE structures with variable spatial orientation and order parameter due to the shear forces acting during the extrusion process. Literature contains various simple 2D LCE structures, such as spiral and radial alignments in disks, which exhibit intriguing shape-morphing capabilities. However, an understanding of complex LCE orientations is yet to be achieved to get extreme shape morphing, snapping and locomotion. In this study, we design structures with complex print patterns by developing custom G-Codes. We prepare a standard LCE ink by mixing the mesogen, RM- 82, cross-linker, n-Butylamine, and a photoinitiator, HHMP, and oligomerizing the mixture at high temperatures. To reduce the temperature-dependent viscosity of the ink during printing, we fabricate an in-house syringe heater that uniformly heats the ink. UV curing was performed during and after printing to fix the director orientation. We first printed several unidirectional rectangular specimens to characterize the effect of nozzle velocity and syringe pressure on the actuation stretch. Higher printing velocities and pressures result in greater shear forces, which produce higher actuation shrinkage. We also found that the shrinkage increases with the actuation temperature. More complex shapes such as a disk with spiral print pattern were printed, which actuates from a planar disc to a 3D cone, due to circumferential shrinkage and radial expansion. We also computationally simulated bilayer structures that can snap to a new configuration and instantly release energy in this process.

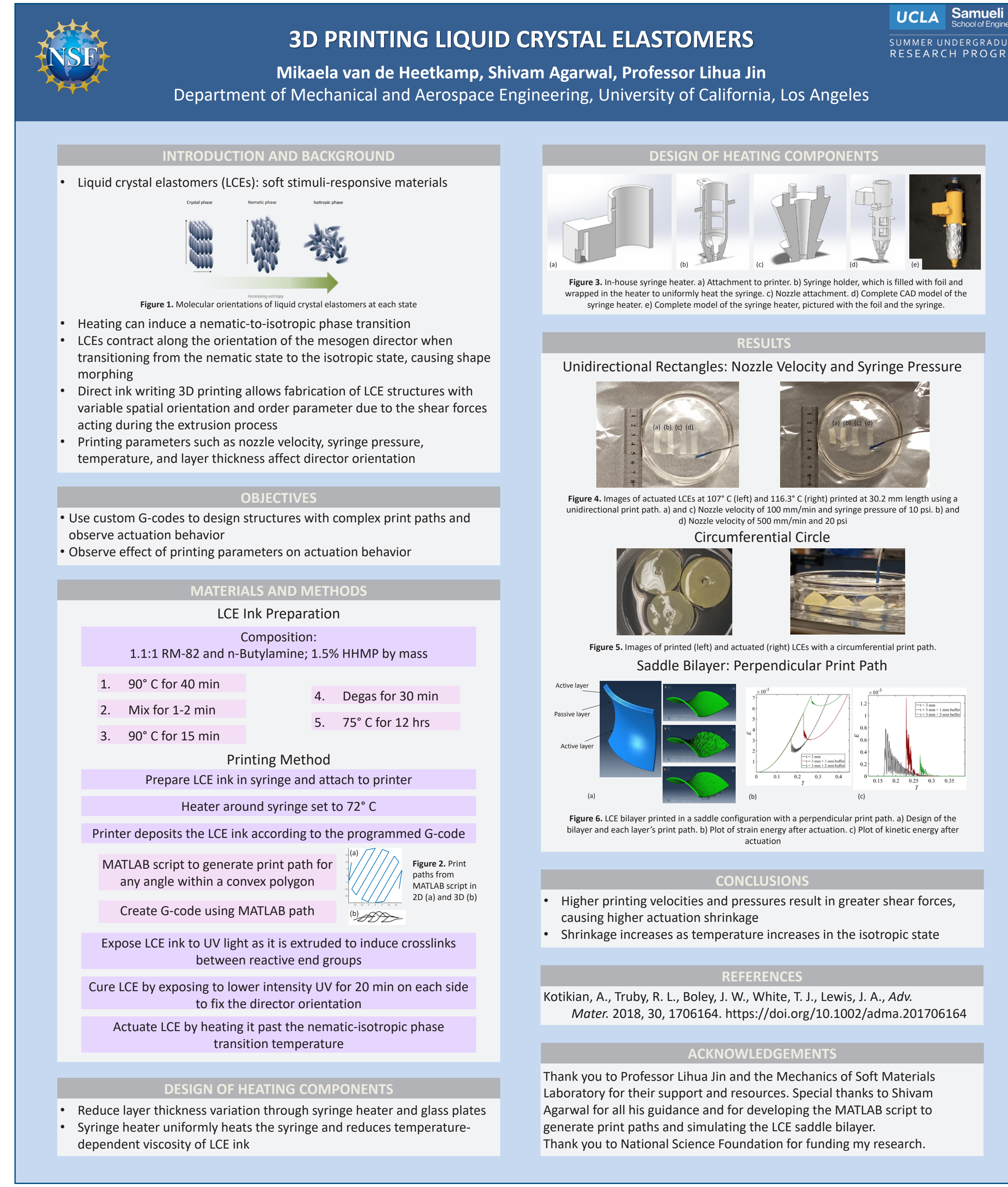

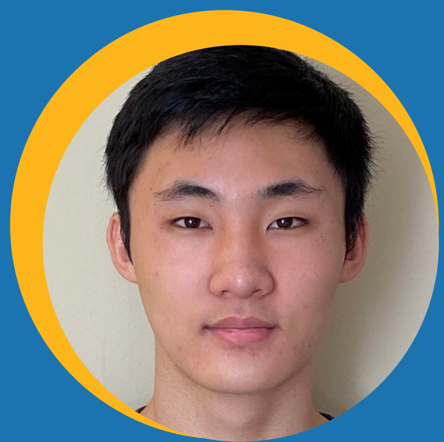

FACULTY ADVISOR
Danijela Cabric

DAILY LAB SUPERVISOR
Tianyi Zhao

DEPARTMENT
Electrical and Computer Engineering

DANIEL YANG

Electrical and Computer Engineering

1st Year, UCLA

Fingerprinting RF Devices

ABSTRACT

Common methods of radio frequency (RF) device authentication, such as RFID tags, cost time or energy. An ideal authentication scheme identifies transmitters from data collected in situ. We investigate such a scheme here. Due to hardware imperfections, identically manufactured RF devices transmit slightly different signals. We attempt to extract this discrepancy for use as a fingerprint. A dataset was created consisting of data collected from seven transmitters sending WLAN packets to one receiver. Since wireless channels can distort these transmitter fingerprints, we also introduced the effects of seven different channels on the signals. The received short and long training fields were extracted and used as input to train a neural network to classify the transmitters and evaluate the effect on accuracy of the channels. Further work may be aimed towards eliminating channel distortion.

FINGERPRINTING RF DEVICES

Daniel Yang, Tianyi Zhao, Professor Danijela Cabric
ECE Department, UCLA; CORES Lab

UCLA Samueli School of Engineering
SUMMER UNDERGRADUATE RESEARCH PROGRAM

INTRODUCTION

Wireless communication involves a transmitter sending signals to receivers. Security is a rising issue as the number of radio devices in the Internet of Things (Iot) increases. Determining which transmitter sent a signal is called classification and is an important step to ensure that only known transmitters are allowed to transmit on a network. Classical authentication methods, such as username/password schemes, take time and energy. Ideally, authentication happens in situ and automatically, with minimal energy and time costs.

BACKGROUND & GOAL

Radios manufactured using the same process possess slight hardware differences, due to tolerances in components such as resistors. As a result, identical signals sent by identically manufactured radios have slight differences.

The goal of this project is to extract these discrepancies and use them to train a neural network to classify transmitters.

METHODS

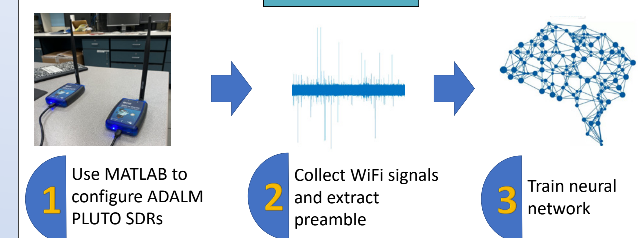

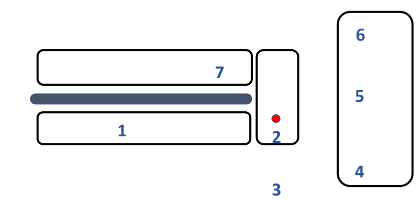

Left: Transmitter (red dot) and receiver (numbered) locations.

RESULTS

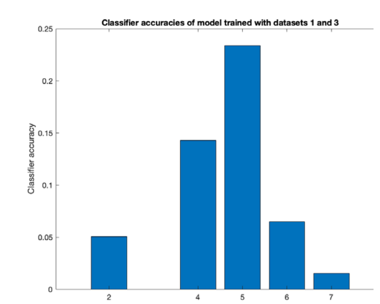

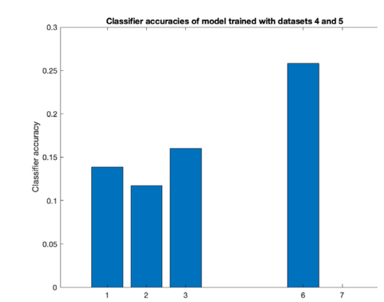

- **Classifier accuracy** used here refers to probability of the training model in correctly deciding which transmitter a signal set was sent by. For example, when trained with datasets 4 and 5, the model correctly identifies signals sent from transmitter 6 roughly 25% of the time.
- Classifier accuracy is lower for channel 2. In this case, the receiver and transmitter are placed close enough together to cause signal saturation.
- Classifier accuracy is also lower for channel 7. This is the only channel in which there is no line of sight from the receiver to the transmitter. This channel therefore introduces more noise than in other channels.
- Other channels have higher accuracy, but are not yet at accuracy levels suitable for transmitter authentication.

CONCLUSIONS & FUTURE WORK

Longer, noisier wireless channels negatively affect classifier accuracy.

This dataset only contains data from 7 transmitters sending to 1 receiver. A clear next step is to develop a larger and more robust dataset of signals collected over many days using more transmitters and receivers.

Another possible direction concerns the effects of channels. In this dataset, the only fact known about the channels is that they are different. In future datasets, it might be of interest to introduce channels in a more controlled way to allow for easier analysis of their effect on the training model, as well as attempt to equalize channel noise.

REFERENCES

- S. Hanna, S. Karunaratne, and D. Cabric, "Open set wireless transmitter authorization: Deep Learning Approaches and dataset considerations," *IEEE Transactions on Cognitive Communications and Networking*, vol. 7, no. 1, pp. 59–72, 2021.

ACKNOWLEDGEMENTS

I would like to thank Professor Gregory Pottie's NSF REU for funding my research during the UCLA Summer Undergraduate Research Program. I would also like to thank Professor Danijela Cabric and the CORES lab, and especially Tianyi Zhao and Shamik Sarkar, for their guidance and support.

ROBERT YANG

Materials Science and Engineering

3rd Year, UCLA

FACULTY ADVISOR

Aaswath Raman

DAILY LAB SUPERVISOR

Jyotirmoy Mandal

DEPARTMENT

Materials Science and Engineering

Characterization of a Radiative Emitter

ABSTRACT

Materials that passively cool themselves are of particular interest in our society, particularly with the rise of climate change. Since air conditioning actively requires energy to operate and no process is 100% efficient, air conditioning temporarily cools an internal environment at the expense of the world at large. As such, alternative cooling methods are needed that are less energy-intensive. Prior research has demonstrated that materials can be engineered such that they experience a net loss of heat to the cold of space. However, this effect requires a clear view of the sky and minimal view of the ground, conditions rarely met in urban environments. In this experiment, we characterize a directional emitter designed to exhibit high emittance in the 0-180° azimuthal angles about its normal axis, and high reflectance elsewhere. Our samples were tested with a thermal camera at different angles of incidence with respect to a cold background and the resulting temperatures were recorded.

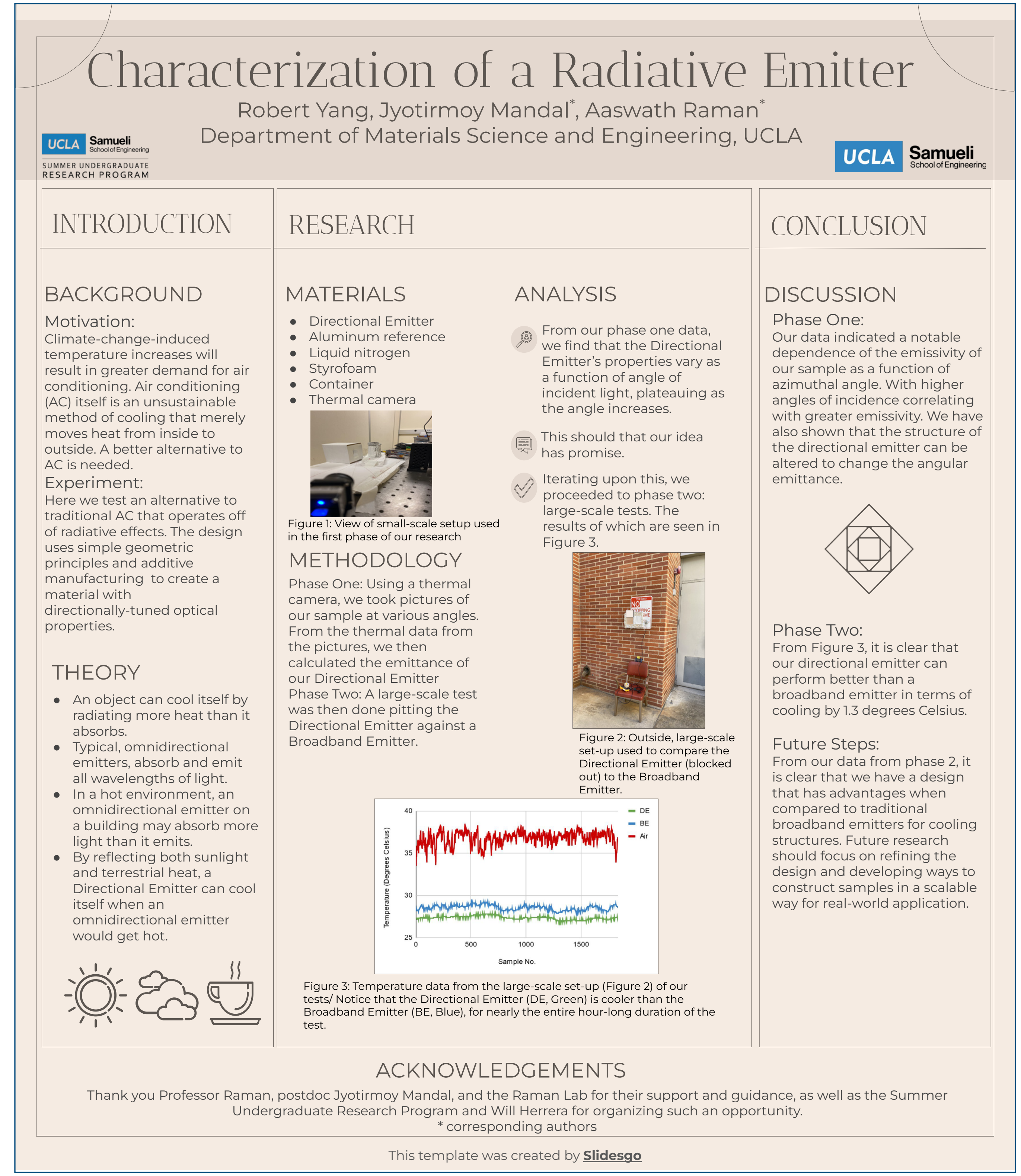

TIANYUE YU

Chemical and Biomolecular Engineering

4th Year, UCLA

FACULTY ADVISOR
Samanvaya Srivastava

DAILY LAB SUPERVISOR
Fahed Albreiki

DEPARTMENT
Chemical and Biomolecular Engineering

Adhesion Characterization of Hydrogels For Wound Dressing

ABSTRACT

Hydrogels are three-dimensional polymer networks that are crosslinked using various chemical or physical crosslinkers and are attractive candidates for medical applications such as wound dressing and tissue engineering. Gelatin methacryloyl (GelMA) is a widely studied hydrogel for tissue engineering due to its similarity to native extracellular matrices. Methacrylate modification of gelatin allows this hydrogel to be covalently crosslinked upon exposure to ultraviolet light leading to robust mechanical stiffness. However, this application has been limited due to its weak mechanical strength before crosslinking, leading to undesired flows on wet surfaces. We propose to overcome the low mechanical strength of GelMA by incorporating oppositely charged block polyelectrolytes (bPE) that self-assemble ionically when mixed in aqueous mediums, resulting in hybrid hydrogels with higher mechanical robustness prior to photocuring. To quantify hydrogel's mechanical properties, we built an ASTM F2392 – 04 standard burst pressure apparatus to measure the maximum pressure that hydrogel acquires to burst. We compared the burst pressure of GelMA with varied concentrations as well as block polyelectrolytes supplemented with GelMA (bPE-GelMA) systems in dry and wet environments. The results showed that increasing GelMA concentration from 5 wt.% to 10 wt.% doubled the burst pressure. In underwater environments, GelMA solutions undergo significant declines in burst pressure. The burst pressure of bPE-GelMA system is nearly equal to the burst pressure in dry environments, showing controlled application underwater compared to rapid dilution of GelMA. This work assessed hydrogel applications and relevant mechanical properties in environments that resemble physiological conditions.

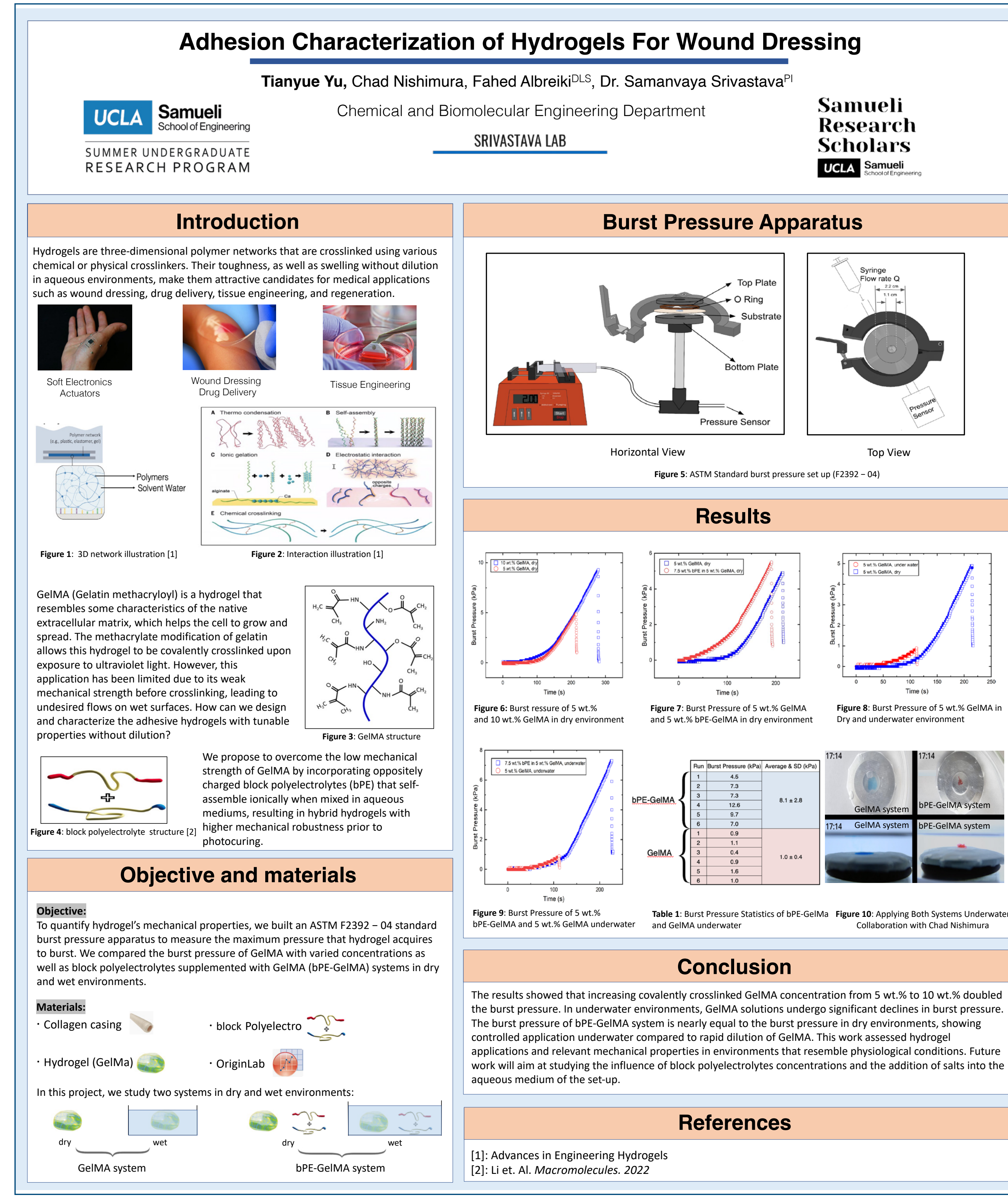

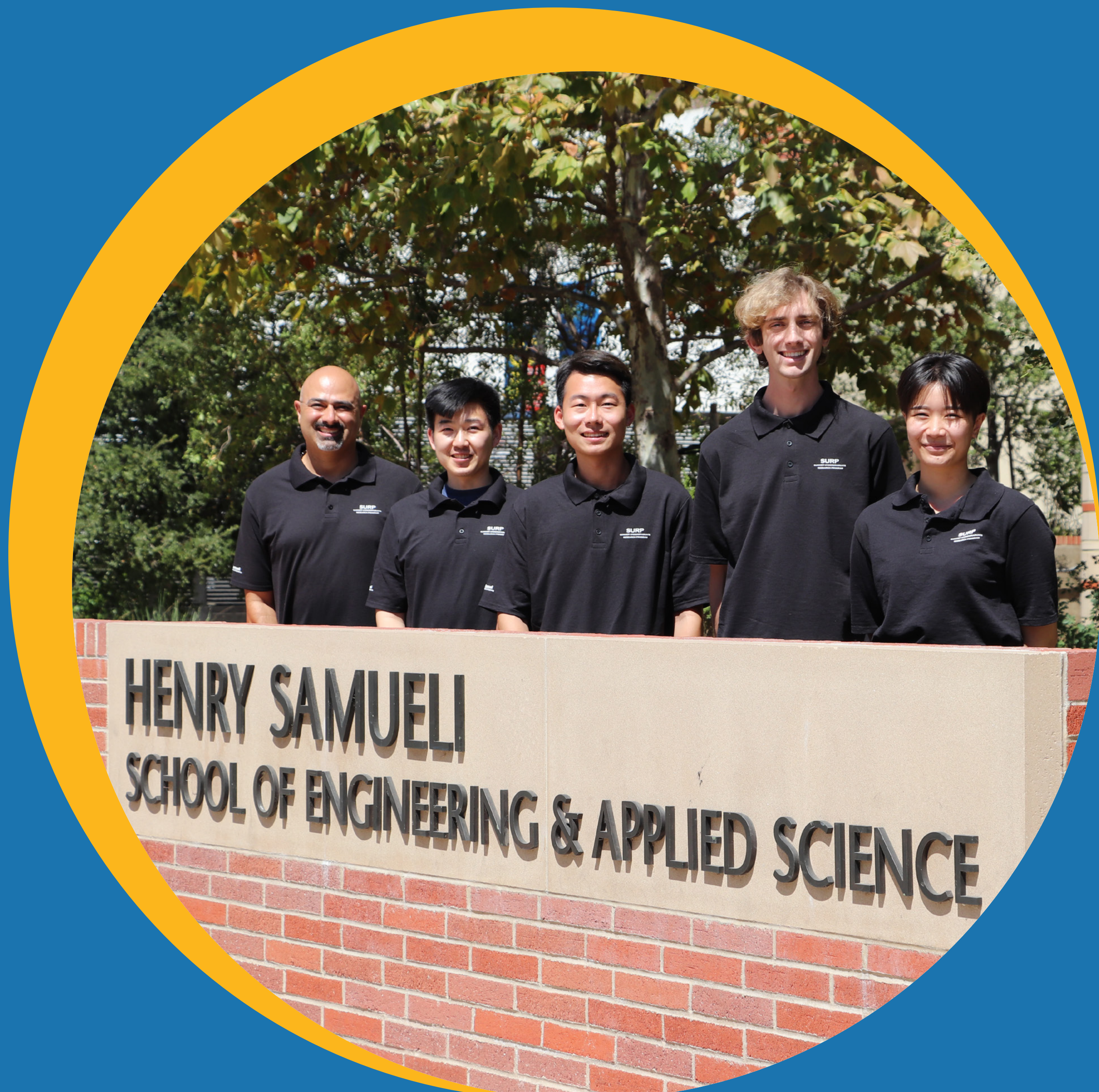

If you would like to find out more about the UCLA Samueli Summer Undergraduate Research Program, please contact our team at surp@seas.ucla.edu or visit our website at www.seasoasa.ucla.edu/surp.

UCLA Samueli
School of Engineering

UCLA Samueli
School of Engineering

UCLA Samueli Summer Undergraduate Research Program
Office of Academic and Student Affairs
UCLA Samueli School of Engineering
420 Westwood Plaza, 6288 Boelter Hall, Los Angeles, CA, 90095-1600
310.825.9478 | www.samueli.ucla.edu